# ME40346: Major Individual Design Project

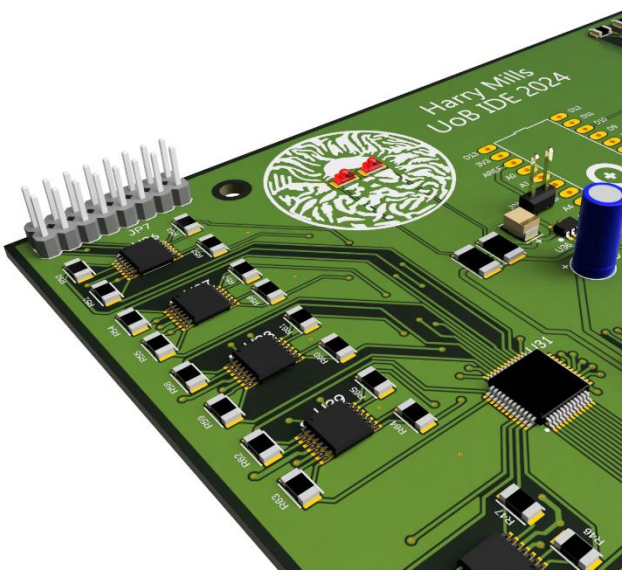
Final Design Report





# Design of a Pressure Sensing Array for the Inflatable Prone Repositioning Device (IPRD)





Harry Mills (12196)

**Supervisor**: Alexander Lunt

**Assessor**: Ioannis Georgilas

Word count: 10,381

01-May-2024

# Summary

This report details the development of a pressure sensor mat to be integrated with the Inflatable Prone Repositioning Device (IPRD) or BathMat. This project builds on two previous years of MIDPs which worked in collaboration with Royal United Hospitals (RUH), Bath, to develop the IPRD vessel. The IPRD makes repositioning proned ICU patients faster and less-labour intensive for doctors and nurses, allowing more frequent repositioning, which in turn reduces the incidence of pressure sores.

The need of a pressure sensor mat in a medical context was primarily to evaluate whether the IPRD would exacerbate pressure sore formation by creating pressure concentrations when deflated, but also to provide doctors and nurses with valuable real-time data about the locations of pressure points so they can reposition patients more effectively and hopefully reduce the incidence of pressure ulcers. However, as a further demonstration of the value of pressure sensor data, it was also desired to be able to autonomously control the IPRD pneumatic valves by using live pressure sensor data feedback to automatically reposition a person lying prone on the IPRD.

In a business context, pressure sensor mats are not unique, but large-scale commercial sensors similar to the prototype developed for this project are expensive (£7000-£10,000) due to high-tech specifications and catering to a small niche market. In order to promote widespread adoption of this technology, a low-cost implementation of pressure sensor technology was desired that could provide useful real-time data to bedside staff.

Ultimately, the prototype developed for this project successfully displayed a real-time map of pressure across a  $70 \times 70$  cm area at a resolution of 14 mm/cell, with a scanning rate of 1 Hz. The sensor mat was < 2 mm thick, introduced no hard or rigid objects to the sensor surface, and was fully flexible. Automatic repositioning using pressure sensor data feedback to the pneumatic control was also successfully demonstrated. Overall, the full-size prototype produced in this work cost £247, an insignificant amount compared to commercial sensor mats with similar resolution and size. Thus demonstrating that low-cost technologies could be applied to generate valuable pressure mapping data which is usually not widely available to healthcare professionals due to the associated cost.

Finally, a number of suggestions for developing the prototype beyond this project have also been suggested. Developments to the sensor electrodes, a biocompatible waterproof casing, and implementation calibration methods are key to advancing this project technically and working towards full integration with the rest of the IPRD.

## **Contents**

Sur	nma	ry	ii
1	Intr	oduction	1
1	.1	Problem Statement	2
1	.2	Market Opportunity	3
1	.3	Summary of Previous Work	4
1	.4	Concept Architecture	12
1	.5	Prototype Specification	13
2	Dig	gital Acquisition Hardware (DAQ) Development	15
2	2.1	Cross-talk Reduction	15
3	Sof	tware Development	25
3	3.1	Arduino Code	25
3	3.2	Visualisation Code	28
4	Pne	eumatics Development	30
2	l.1	Pneumatic Hardware	30
4	1.2	Pneumatic Software	31
5	Ele	ctrode Development	33
5	5.1	Initial Prototype Mat	33
5	5.2	Full-size Prototype	34
5	5.3	Screen Printed Design	36
6	Ful	l System Testing	39
6	5.1	Pneumatic Integration	40
6	5.2	Final BOM	41
7	Coi	nclusions & Future Work	42
7	7.1	Future Improvements	43
7	7.2	Final Conclusions	47
Ref	eren	ces	48
Ар	pend	lix A: PCB Design Documents	52
Ар	pend	lix B: Row Control Logic Truth Table	56
Ар	pend	lix C: Arduino ADC Clock Pre-scale Modification	57
Ар	pend	lix D: Screen Printed Electrode Design	58
Api	pend	lix E: Prototype System Bill of Materials	59

# **Abbreviations**

IPRD Inflatable Prone Repositioning Device

ARDS Acute Respiratory Distress Syndrome

NHS National Health Service

PP Prone Position

PU Pressure Ulcer

ICU Intensive Care Unit

MCU Microcontroller

MUX Multiplexer

IC Integrated Circuit

ADC Analog to Digital Converter

MVP Minimum Viable Product

## 1 Introduction

Acute Respiratory Distress Syndrome (ARDS) is an acute, inflammatory type of lung injury which can be life-threatening for seriously ill patients. ARDS is usually a complication of another serious condition (e.g.: COVID-19 or pneumonia) and causes significant lung damage, fluid accumulation, and reduced oxygenation to the bloodstream [1]. ARDS is a life-threatening condition and cannot always be cured. Mortality is proportional to the severity of the disease: 32% in moderate cases, and 45% in severe cases of ARDS [2].

Patients with ARDS are treated with supplementary oxygen, or in more severe cases via mechanical ventilation [3]. Additionally, patients are often placed in the prone position (lying on their front), as this has been shown to improve oxygenation of the blood and improve fluid drainage from the lungs, leading to reduction in mortality of 17% compared to non-proned patients. However, ARDS patients can spend up to 20 hours a day in the prone position unable to move themselves since they are unconscious. NHS guidelines suggest proned patients should be repositioned every 2–4 hours to avoid formation of pressure ulcers or nerve injuries [4]. Repositioning requires 5-6 medical staff around 30 minutes to complete, so during high demand (such as during the COVID-19 pandemic) this becomes very labour intensive for ICU staff.

To combat this, the Inflatable Prone Repositioning Device (IPRD) has been developed over the last two years as part of Anders Vangsgaard and Luke Ortleib's Major Individual Design Projects. The IPRD (Figure 1) is a wedge-shaped inflatable vessel that is placed under a proned patient's torso and inflated to make the repositioning process less labour-intensive, requiring less than 10 minutes for 2 nurses. The IPRD allows safer and more frequent repositioning which is crucial for reducing the incidence of pressure ulcers (Figure 2).



Figure 1 Left: CAD model of the IPRD. Right: CAD model of the IPRD control box

#### **Pressure Ulcer Formation Estimate**

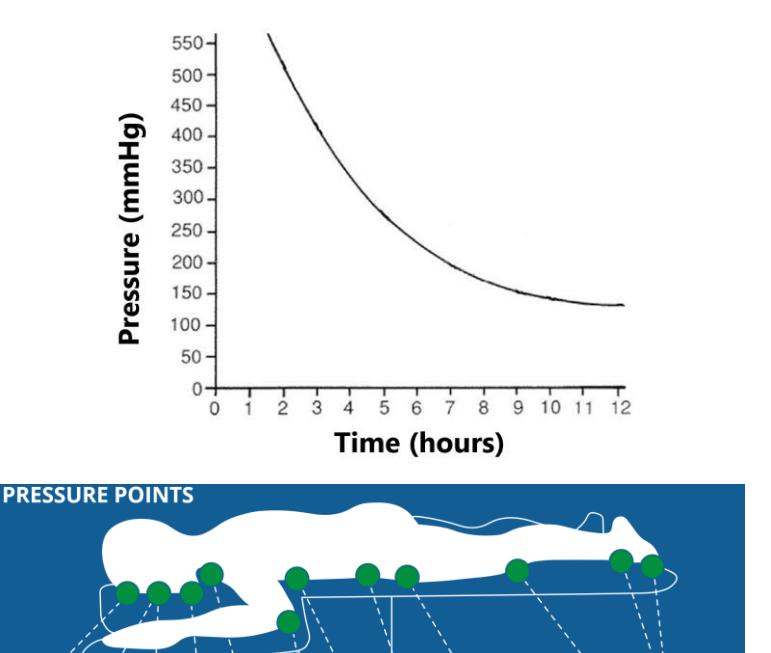


Figure 2: Top: Kosiak's model of skin pressure vs. time to show how long it takes pressure ulcers to form [5].

Bottom: Location of common pressure ulcer formation hotspots when in the prone position [6]

### 1.1 Problem Statement

Pressure ulcers are one of biggest sources of litigation against the NHS and treatment costs an estimated £1.4 - £2.1 billion annually in the UK [7]. During high demand (such as during the COVID-19 pandemic) repositioning is not done regularly enough to prevent pressure ulcer formation in some cases. The IPRD aims to alleviate this problem by reducing staff number and time requirements for repositioning. However, doctors have also requested pressure mapping functionality with the IPRD. This would show where pressure points are for more effective repositioning, or ideally through automated closed-loop control of the IPRD vessel pneumatics to constantly reposition the patient to avoid pressure ulcers forming.

This project focuses on developing pressure distribution mapping technology to be integrated with the IPRD to provide live pressure data to bedside staff. Firstly, this data will confirm the IPRD does not create excessive pressure points when inflated and uninflated which may lead to pressure ulcers forming. Also, this data can be displayed live to healthcare workers to help them evaluate potential areas at higher risk of pressure ulcer formation to improve the effectiveness of repositioning. Finally, using live pressure distribution data to control the IPRD pneumatics via automatic feedback can also be explored as a way to reposition patients automatically and constantly by inflating different parts of the vessel based on the measured pressure distribution.

Commercially available pressure sensor mats are very expensive (£7000-£10,000), so implementing this technology in a low-cost way is key to enabling more widespread uptake of the technology – as current usage is limited to specialist testing and development purposes.

# 1.2 Market Opportunity

The problem statement can be reformulated into a market opportunity statement (Table 1). This defines what user needs the product aims to meet and the benefits of developing and implementing this technology.

Table 1 Market opportunity for a low-cost pressure mapping mat

Pressure Sensor Mat Market Opportunity								
<b>Product Description</b>	Low-cost, thin, flexible pressure sensor mat to be used on a hospital bed.							
	Provide healthcare workers with live pressure distribution data so they can reposition patients more effectively.							
Benefits	Pressure data can be used in a closed feedback loop to control air distribution under the patient to automatically reposition.							
	Low-cost technology will allow wider uptake of the technology across the NHS, impacting more patients.							
Business Goal	Widespread use of pressure mapping technology to help healthcare workers reduce the incidence of pressure ulcers.							
Market	NHS: ICU wards where patients lie unconscious in the same position for extended periods of time, and commercially available pressure sensors are not cost effective.							
	Other settings where people are sedentary for extended periods – care homes or car/train seats for example.							
	Nurses/Doctors							
Stakeholders	Patients							
	IPRD development team							

## 1.3 Summary of Previous Work

The initial project brief was to develop a pressure sensor mat to be integrated with the IPRD. Work in Semester 1 (Oct - Dec 2023) focused on researching the background of pressure sensing technology and evaluating potential sensor architectures which would be developed during the prototyping phase (Feb – Apr 2024). Mini-study 1, 2 and the Design Specification report are attached in the Supporting Documents folder for reference.

## 1.3.1 Mini-Study 1

Mini-study 1 compromised a literature review exploring the range of pressure sensing technologies available to measure 2D pressure distributions. Commercially available pressure sensor arrays were also analysed to understand current uses, common design features, and establish a target specification.

Table 2 summarises the range of sensor architectures that can be used in this application with positives and negative evaluated based on the IPRD brief and the context of usage within an ICU environment.

Table 2 Comparison of pressure array sensor architectures with respect to the IPRD project brief requirements

Sensor Architecture	Measured Parameter	Advantages	Disadvantages
Piezoresistive	Change in resistance	High spatial resolution High matrix scan rate Flexible & unobstructive Durable Low cost Humidity/water unaffected	Susceptible to drift Poor response to high frequency vibrations Low repeatability
Change in capacitance		Excellent sensitivity Good spatial resolution Large dynamic range Low power consumption Flexible & unobstructive Long-term drift stability	Water/humidity affects performance EMI Noise susceptible Poor hysteresis effects
Optical	Light intensity	Fast scanning system response Very high spatial resolution Lightweight High repeatability Immune from EMI	Contains rigid and bulky light emitters and detectors
Piezoelectric	Change in voltage	Widely used for vibration sensing High frequency response High sensitivity	Limited to dynamic measurements Susceptible to temperature changes

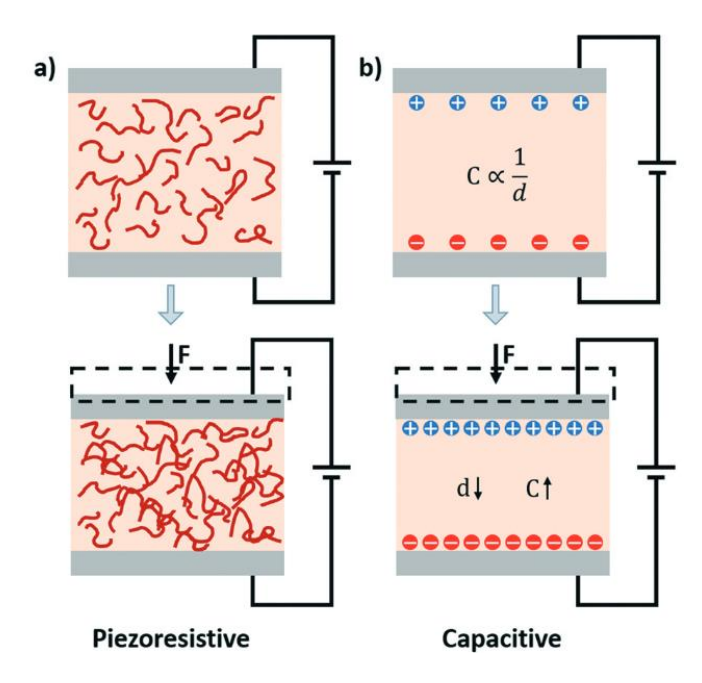


Figure 3 Schematics showing the main mechanisms of force transduction in pressure sensors[8]

The key driving requirements from the initial brief were that the selected sensor must be flexible, thin, and not introduce rigid components or sources of pressure concentrations, as well as having a good enough resolution to detect localised pressure points. The most suitable sensor architectures were found to be capacitive or piezoresistive (Figure 3) as these provided the most flexibility, low-cost construction, and good spatial resolution without being too complex or bulky. Optical and piezoelectric sensors were found to not meet the criteria for the IPRD brief, being either not flexible, having rigid components or not suitable for static measurements. Through further research, a piezoresistive sensor was identified as the most suitable architecture with respect to the IPRD project. The key benefits over capacitive sensing are that measurements are unaffected by water or humidity (which may be present in ICU settings), cheaper prototyping materials and less complex electronic processing. Although, capacitive and piezoresistive sensors commercially provide very similar data, so further development beyond this project could consider both sensor systems.

Table 3 Comparison of commercially available body sized pressure sensor arrays [9 - 11]

Attribute	XSENSOR Foresite PT	Tekscan BPMS	SPI Tactilus Bodyfitter
Sensing technology	Capacitive	Piezoresistive	Piezoresistive
Cost	>\$10,000[12]	>\$10,000[12]	N/A
Scan frequency	10 Hz	60 Hz	50 Hz
Drift	5%/hr @ 100 mmHg	5%/hr @ 100 mmHg	-
Spatial resolution	10 mm	10 mm	25 mm
Sensor range	5 – 200 mmHg	0 - 300 mmHg	0 - 100 mmHg
Hysteresis	8%	4.5%	5%
Size	1880 x 760 mm	1950 x 850 mm	1850 x 760 mm

Analysing hospital bed sized commercial sensor arrays showed that their extremely high cost is the reason for lack of widespread utilisation of pressure mapping technology. Commercial pressure sensors are piezoresistive or capacitive systems and often cost over £10,000 for body pressure mapping applications [12, 13]. Currently, there are not enough benefits of implementing this technology to justify the cost of implementing it in ICUs nationally. Table 3 summarises commercially available body-sized pressure sensor arrays which could be used for this task, but as mentioned they are excessively expensive and over-specified for the project.

Encouraging more widespread usage of pressure mapping technology can be improved firstly by increasing the value-added - using pressure data for closed-loop feedback was not identified in any commercial product and is discussed minimally in literature [14]. Informing the nurses how, where and when to reposition, or ideally automatic constant closed-loop pneumatic repositioning, is valuable for healthcare workers to increase patient quality of care without much increase in material cost or complexity. Secondly, by implementing the technology for a lower cost at the expense of non-critical performance such as high refresh rates (>10 Hz), and very high spatial resolution (<10 mm) allows cheaper construction while still delivering useful data [15].

#### 1.3.1.1 Outcomes

The outcome of Mini-study 1 was a high-level ideal product specification (Table 4) to meet the needs of the brief, based on analysis of available technology and commercially available solutions that meet the needs of the brief.

	Requirement	Demand/Wish	Source
1	Flexible, thin and unobtrusive construction	Demand	[10], [16]
2	Sterilisable container/outer surface	Wish	[17]
3	Fits within an NHS hospital bed (900 x 2000 mm)	Demand	[16]
4	Visual feedback of localised pressure points	Demand	[10], [11], [18]
5	Integrate sensor array into IPRD surface	Wish	[11]
6	Closed-loop feedback to control IPRD inflation from surface pressure distribution	Wish	[14]
7	Low cost (<£150)	Wish	[12], [17], [18]
8	0.5hz refresh rate	Demand	[10], [11]
9	0 – 100 mmHG pressure range	Demand	[10], [11]

Wish

[9], [10]

Table 4 Draft design specification after completing mini-study 1

## 1.3.2 Mini-Study 2

25mm sensel resolution

10

Build on research in Mini-Study 1, the second research stage involved building and testing a simple proof of concept prototype pressure sensor array. This demonstrated how the piezoresistive effect used by many sensors in literature and commercially can be applied using low-cost materials. Going forwards, it highlighted key design directions for development that could be improved on before moving on to larger full-scale prototype pressure sensors.

Figure 4 shows the prototype piezoresistive sensor matrix created. This was constructed from 2 sets of horizontal copper tape electrodes on a paper substrate with a piece of Velostat [19] (piezoresistive material) sandwiched in between to form a 7 x 7 grid of sensing points.

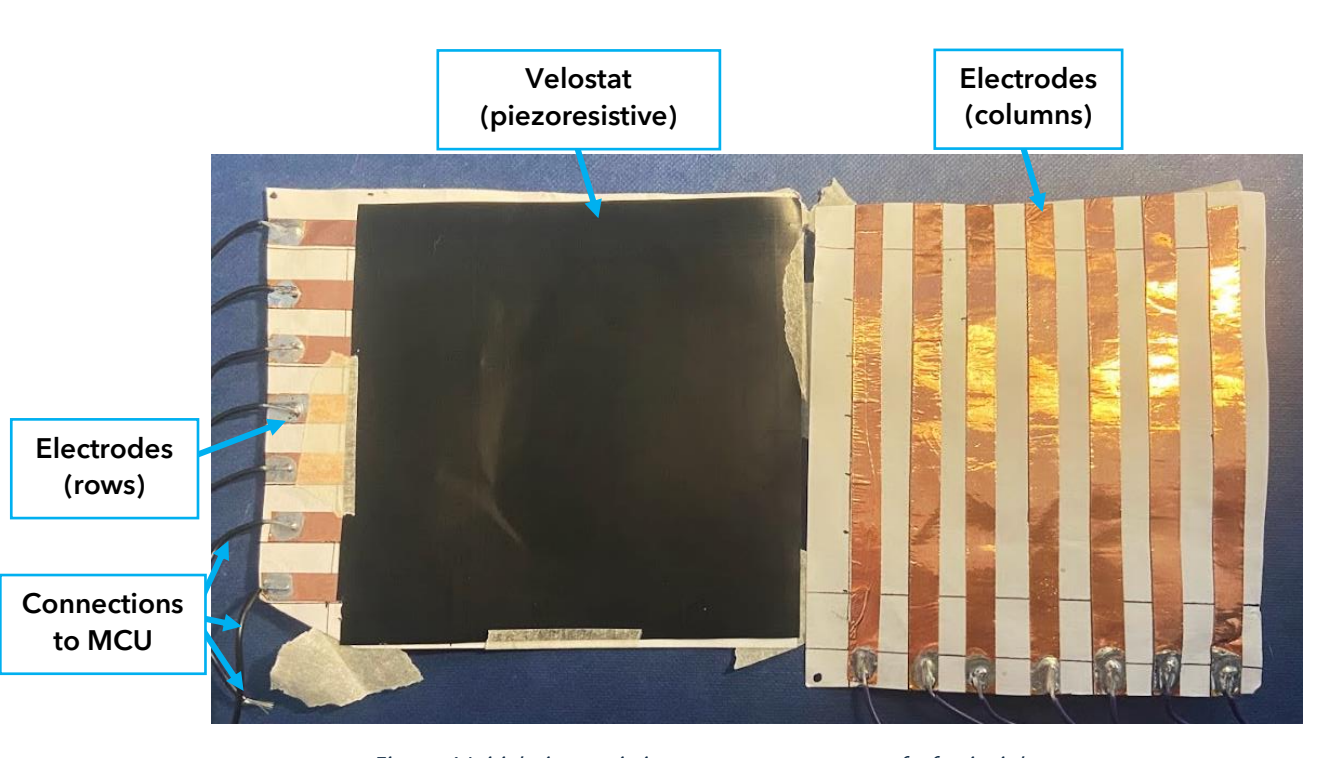


Figure 4 Initial piezoresistive pressure sensor proof-of-principle prototype

This is a 'passive matrix' array, where the individual sensing cells are not addressed by the interface electronics directly – rather for a certain row each column is measured one at a time. Directly addressing each sensor is a simpler system but does not scale well with the number of sensors. For M rows by N columns, directly addressing sensors requires 2xMxN connections, whereas a passive matrix requires M+N [20]. For example, the commercial sensors in Table 3 have 190 columns and 75 rows, requiring 265 connections in a passive matrix, but over 20,000 connections if each sensor was addressed directly. Therefore, a passive matrix array is necessary to be able to connect to and take readings from a pressure sensor with the size and resolution requirements of the IPRD [21, 22].

This prototype was made to test the principles and function of a passively addressed piezoresistive pressure sensor, so paper and masking tape were used to bond the layers together, with future iterations considering material choice more carefully.

### 1.3.2.1 Initial Prototype Operation

Figure 5 shows the software flowchart required to drive the pressure sensor array from an Arduino Nano Microcontroller (MCU) and display it as a live-updating pressure matrix. Each row of the matrix is connected to an Analog voltage reading pin, while each column is connected to a digital output (High or Low voltage). Figure 6 shows a simplified schematic of this to demonstrate how this creates a voltage divider using the internal Arduino pull-up resistor and the variable resistance of the Velostat [23]. The output voltage read by the Arduino,  $V_{in}$  is 3.3 V from the pulled-up pin, and  $R_1$  and  $R_2$  are the pullup resistor, and Velostat resistance, respectively.

$$V_{out} = v_{in} \left( \frac{R_1}{R_1 + R_2} \right) \tag{1}$$

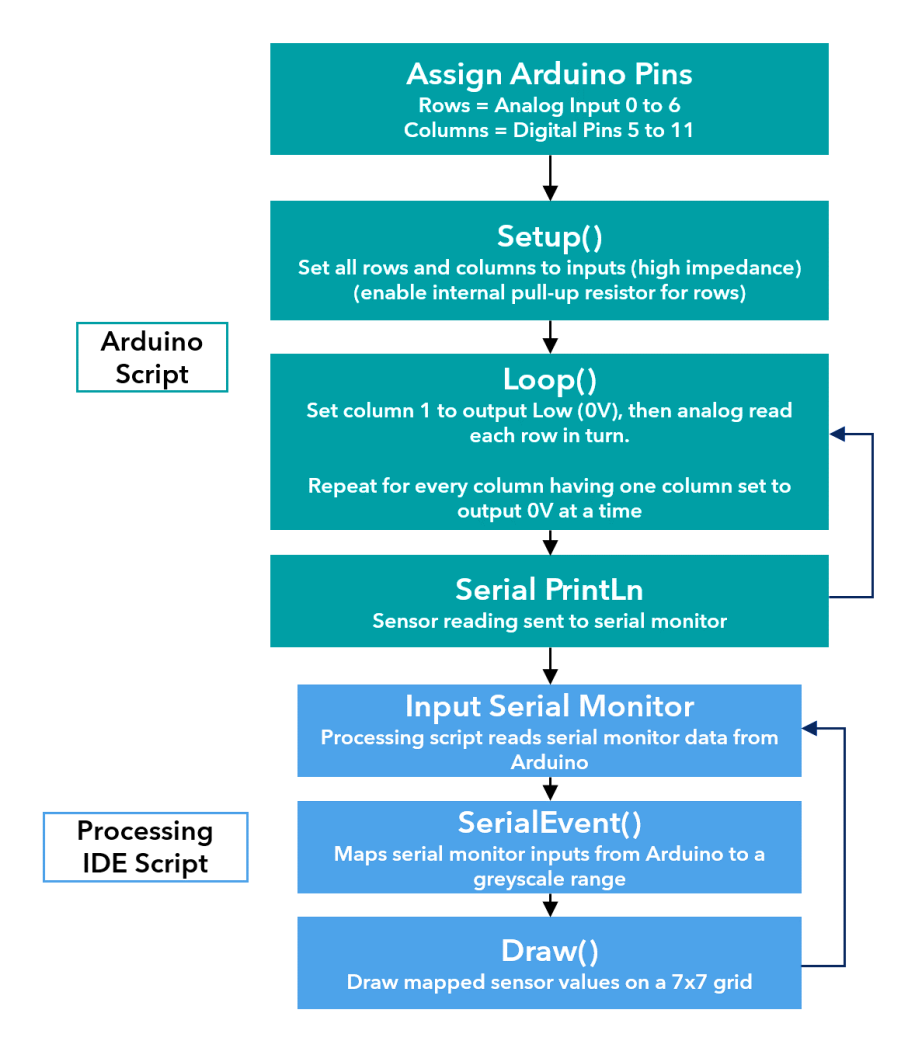


Figure 5 Flow chart of Arduino software to drive the pressure sensor array and Processing IDE script to display to pressure matrix

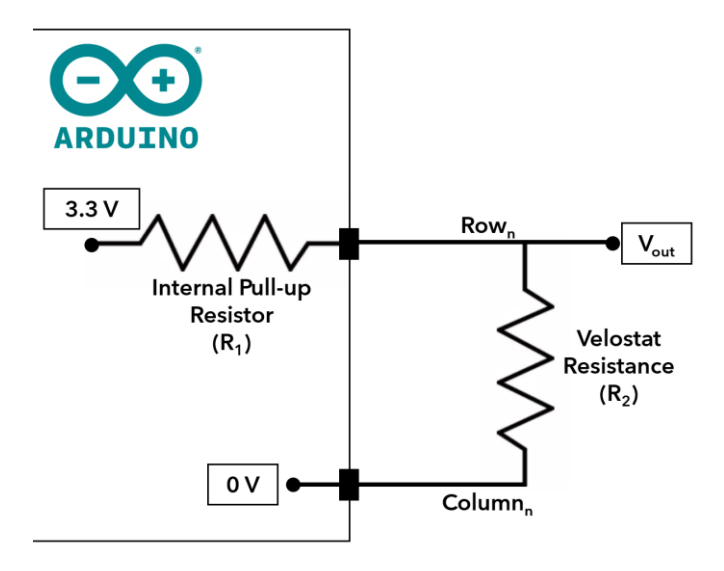


Figure 6 Schematic of voltage divider setup for one sensing cell to measure resistance changes in the Velostat by creating a potential divider

To summarise the process, after the rows and columns are assigned to Arduino inputs and setup, the function loop(), iterates through each column and row to measure voltages. Figure 7 visually shows this loop. Firstly, a column is set to LOW (0 V) (the rest to OUTPUT (high impedance)), and then an analog voltage reading is taken from each row. This is then repeated for every column. Voltage readings are stored in a matrix which is sent to the serial monitor upon reading the whole matrix.

Processing IDE is used to generate a real-time visualisation of sensor data sent over the serial monitor [24], [25]. This maps voltage readings from the Arduino to a greyscale range, and then uses the draw() function to create a live updating matrix showing the pressure at each node. A video of the prototype functioning is attached in the supporting information to this document (see *PrototypeV0.mp4*).

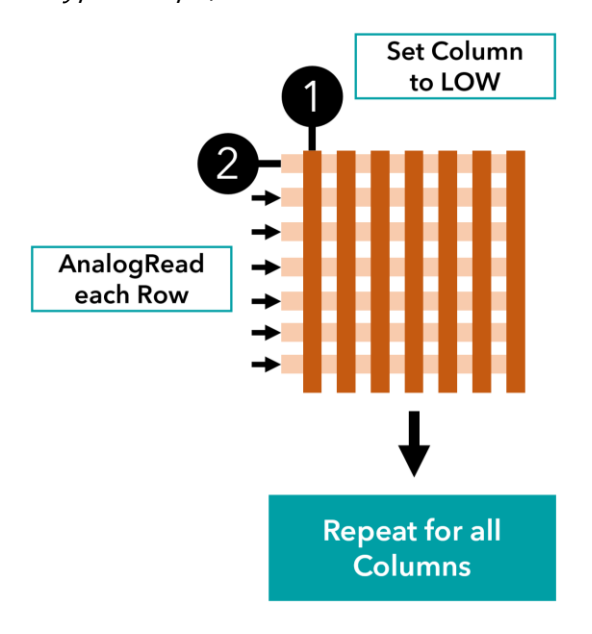


Figure 7 Visual explanation of the loop() function in the Arduino code

#### 1.3.2.2 Problems Identified

The prototype developed in Mini-study 2 is a very rough initial prototype, but it was a useful exercise to highlight unforeseen problems, and guide future development of both the hardware and software.

The first problem observed was 'ghosting' [26], [27] (Figure 8), which manifests as an entire row reading pressure when in reality only one sensor on the row is being pressed. This occurs due to parasitic current pathways in the sensor due to the passive matrix.

Cross-talk means we cannot find the true of any individual sensor, and also means that sensors not being pressed on the same row as ones that are pressed indicate higher pressure than is actually present. A number of solutions to mitigate cross-talk are proposed in literature, involving more complex electronic driving circuits to interface with the sensor—these are discussed further in the development of the sensor electronics and future improvements.

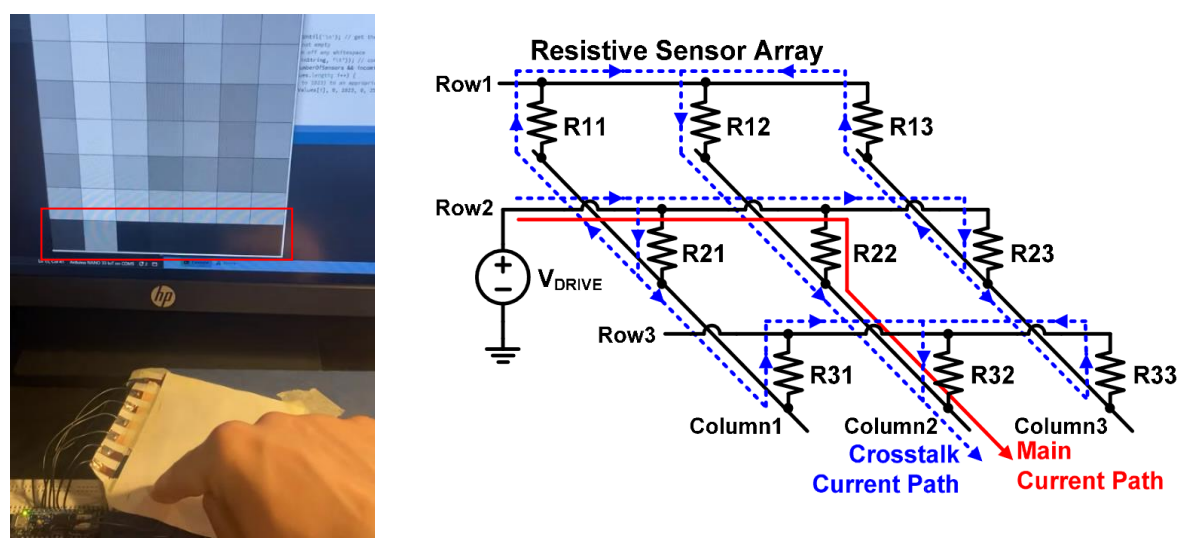


Figure 8: Left: evidence of cross-talk in the prototype pressure sensor array.

Right: Cross-talk is caused by parasitic current pathways in the pressure sensor matrix (Kim et al., 2016 [28])

Another identified issue for further development was the hardware and software interfaces with the matrix. In the hardware, each of the 7 rows was connected directly to an individual Arduino Analog Input pin. The Arduino Nano is based on the ATMega328 microcontroller and has 8 Input channels, so this is already close to the limit. In order to scale the sensor matrix a larger microcontroller could be used, like the ATmega2560 (Arduino Mega) which has 16 analog inputs but is more expensive. Ultimately, the best way to scale the matrix is to use analog multiplexers to switch many rows and columns to a few Arduino pins. A single CD4051 8:1 multiplexer costs £0.28 ([29]), so represents a minor cost even for large sensors.

As the matrix gets increasingly large there is a reduction in performance when addressing the matrix. For the 7 x 7 prototype the refresh rate of the display was not noticeable but scaling this up to a 50 x 50 or larger matrix will reduce this noticeably. The Arduino AnalogRead() command takes ~110 µs to run, which gives a theoretical refresh rate of 180 Hz for a 49-element array, but only 0.6 Hz for a 150 x 100 array.

The final improvement identified in the initial prototype was material choice. Paper and copper tape were used as quick solutions to make the electrode strips, but within a medical setting the final sensor mat would need to be waterproof, flexible, and sterilisable. Part of this could be solved by encasing the sensor in a waterproof nylon fabric or neoprene, but additional layers in between the patient and sensor blur the data by distributing pressure before it is measured – so should be avoided where possible.

# 1.4 Concept Architecture

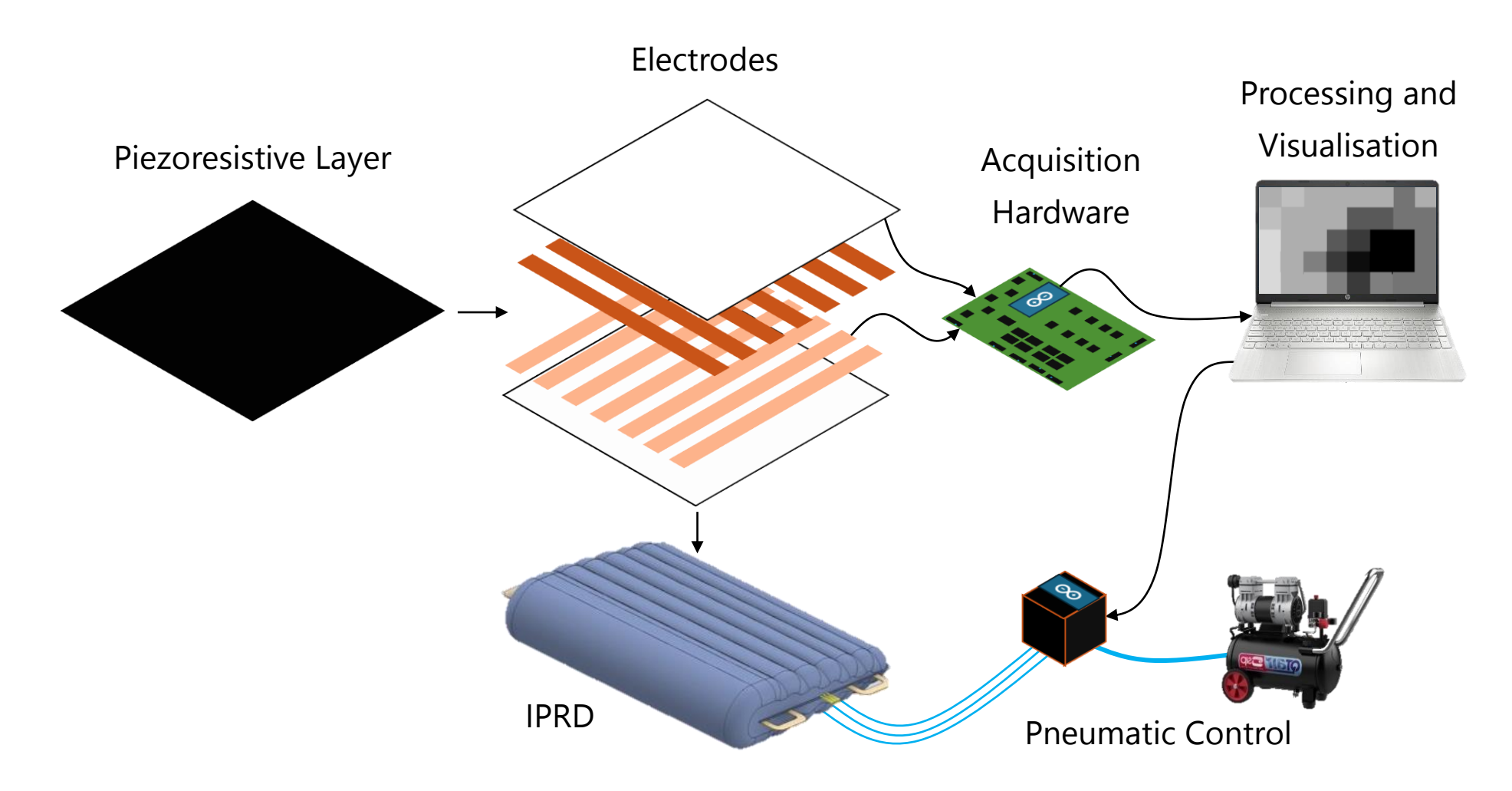


Figure 9 High-level diagram of connections between subsystems of the proposed pressure sensor prototype with pneumatic control

Figure 9 shows a high-level conceptual architecture for the prototype system. The pressure sensor matrix is constructed from sandwiched layers of orthogonal conductive electrodes with a piezoresistive layer in between. The sensor matrix is addressed by an interfacing PCB, which uses a microcontroller to switch between each row and column respectively to sample the entire matrix. Voltage readings from the microcontrollers are sent to a PC for processing displaying visually. The focus of this project is mainly the pressure sensor mat development, but the pneumatic control of the IPRD is also shown. This represents how a feedback loop can be implemented to use the pressure sensor data to redistribute air in the IPRD.

The subsystems which must be developed for this project are detailed in Table 5. The piezoresistive layer was not focused on for this project, Velostat (used in initial prototype) was low-cost and functioned well enough to be implemented in the final prototype.

Table 5 Main subsystems to be developed to demonstrate full system functionalit
---

Subsystem	Function	Report Section
Digital Acquisition Hardware (DAQ)	Expand IO of the microcontroller and drive the rows and read the voltage of columns in the matrix while reducing cross-talk	2
Software	Firmware of the microcontroller to drive the DAQ hardware to read the matrix as fast as necessary.  Visual processing to generate live update display and user interface.	3
Pneumatics	Using pressure sensor data to drive pneumatic valves controlling the IPRD	4
Electrodes	Flexible, thin surface containing rows of parallel conducting strips to create discrete sensing points	5

## 1.5 Prototype Specification

The full product design specification (PDS) is included in the Supporting Documents folder. Each requirement was associated with a design 'stage'. Stage 1 requirements are needed for sub-system validation, stage 2 for MVP (minimum viable product) validation, and stage 3 only for final product validation. Due to the timescale of the project stage 1 and 2 requirements will be the focus of development in semester 2, these are summarised in Table 6.

	Bt	Target Value		Stage		H/M	Comments		Source
	Requirement			2 3 /L		/L	Comments	Evaluation Method	
1. Performance									
1.1	Minimum pressure sensor array spatial resolution	< 80 mm spacing	<b>√</b>	<b>√</b>	✓	Н	Pose recognition ability shown to deteriorate above this value	Verify electrode PCB spacing (ruler/CAD)	[15]
1.2	Pressure sensor covers entire IPRD	800 x 800 mm	✓	✓	✓	Н	Initial testing for IPRD validation may only require this much coverage	Check total sensor prototype dimensions (tape measure/CAD)	[16]
1.3	Pressure sensor array sample rate	> 0.3 Hz	✓	<b>√</b>	✓	Н	Static pose recognition ability shown to deteriorate above this value	Confirm refresh rate is more than once every 3 seconds (stopwatch)	[15][MS2]
1.4	Pressure sensor array accuracy	±5 mmHg (±0.6 kPa)	✓	✓	✓	Н	Determining high pressure (>50 mmHg) more important than exact pressure values	Prototype demonstration, using calibrated weights	[MS1]
1.5	Minimum pressure sensor array cell saturation pressure	> 100 mmHg (13 kPa)	-	<b>√</b>	✓	М	In line with commercial products, over 2x accepted value for pressure ulcer formation	Prototype demonstration, using calibrated weights	[MS1]
1.6	Data output has minimal noise or artefacts that affect true pressure map visibility	Can identify body outline/posture	-	✓	✓	Н	Free from 'ghosting' or crosstalk issues	Confirm that pressure distribution is an accurate live representation without spurious readings	[MS2]
1.7	Pressure sensor array does not introduce hard objects to the IPRD surface	No hard/rigid objects in sensor surface	✓	<b>√</b>	<b>√</b>	Н	Pressure sensor must not exacerbate pressure ulcer formation	User testing to confirm no hard objects are felt during use	[MS1]
1.8	Pressure sensor array is flexible	Pressure mat can measure pressure on non-flat surfaces (IPRD)	✓	✓	✓	Н	Fully flexible pressure sensing surface to conform to the surface of the IPRD	Confirm there is no degradation in performance with repeated use with the IPRD	[MS1]
1.9	Device can automatically reposition based on live pressure mapping data feedback	Closed-loop control of pneumatics achieved	1	<b>√</b>	<b>√</b>	М	Constant repositioning based on closed-loop pressure feedback. More detail on this needed.	Prototype demonstration of closed-loop pressure distribution feedback	Client feedback
2	2. User								
2.1	Live pressure distribution map can be displayed	Real-time display	-	✓	<b>√</b>	Н	Real-time pressure map can be livestreamed on laptop or phone	Prototype demonstration of live data display	Client feedback [16]
2.2	Device provides feedback to indicate pressure ulcer formation risk	Audio-visual alerts to healthcare staff	-	<b>√</b>	✓	Н	Bedside staff are made aware when pressure ulcer risk is increasing, and the patient may need repositioning	Prototype demonstration of alarm/alert when excessive interface pressure is not alleviated	[MS1]
2.3	Device can be switched between manual and automatic repositioning easily	User interface allows mode switch	1	✓	✓	М	Potential safety concern if auto-reposition feedback malfunctions	Confirm button/function to toggle on/off automatic repositioning	[MS1]
3. Life in service									
3.1	Device is modular and sub-systems can be replaced	All sub-systems replaceable	-	<b>√</b>	<b>√</b>	L	Electronics, sensor matrix, and outer casing individually replaceable if a part is broken or must be disposed of.	Device can be disassembled and reassembled non-destructively	Good practice
3.2	Pressure sensor is thin and unobtrusive	< 3 mm total thickness	-	✓	✓	Н	Bulky thick sensor is undesirable	Measure thickness of final prototype	[16]
3.3	Device can be stored easily by one person	Rolled or folder without damage repeatedly	-	✓	✓	М	Investigate best method of storage	Check there is no degradation in performance following repeated folding and rolling for storage	Client feedback

Table 6 Early stage prototype specifications derived from the full product design specification

# 2 Digital Acquisition Hardware (DAQ) Development

Regardless of the electrode design or the piezoresistive material used, any passive array resistive sensor requires interface driving electronics. As stated in Table 5, this must deal with cross-talk and reducing noise, while also expanding the limited IO pins of the microcontroller (to enable use of a low-cost Arduino Nano microcontroller) via analog multiplexing.

For the purposes of this project an Arduino Nano was used due to the simplicity of prototyping and familiarity, however as discussed further in the Future Improvements section there are technically better options such as larger microcontrollers or FPGAs to drive the matrix which should be considered for future developments.

## 2.1 Cross-talk Reduction

As shown in Figure 8, cross-talk occurs in passive matrix sensors such as the initial prototype presented previously, resulting in inaccurate readings and noisy artefacts in the data. Eliminating cross-talk is usually achieved with additional processing and analog switching electronics. Many solutions are addressed in previous literature [27,28]. Inserting a diode or transistor [30,31] for each sensor point in the array theoretically works but introduces rigid components and increases complexity due to additional physical connections. Voltage feedback methods [32,33] can also be used but with reduced effectiveness as the array becomes large.

The most common method of reducing cross-talk is a zero-potential, or balanced readout scanning method shown Figure 10 and detailed in [27,28,34,35]. This uses an operational amplifier for each column. The inverting and non-inverting inputs of the op-amp must be equal due to virtual short characteristics [36], so all columns and rows have the same voltage (0 V) except for the selected row which is V<sub>Drive</sub>. Therefore, current only flows through the resistive sensor elements in the selected row.

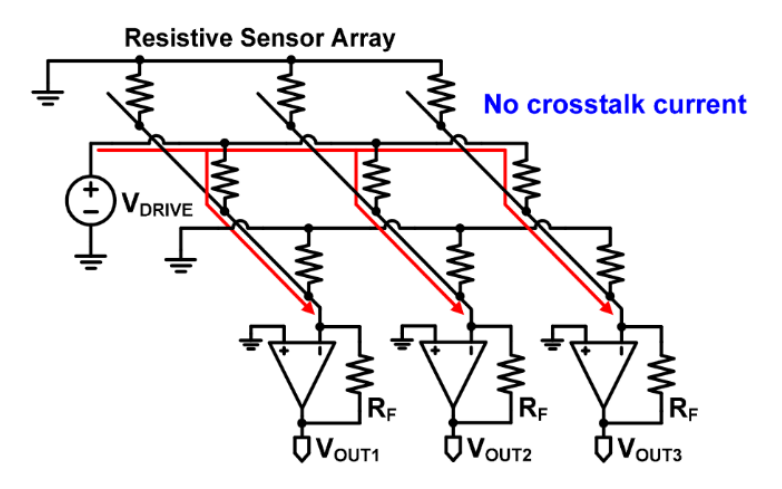


Figure 10 'Zero-potential' sensor driving architecture to eliminate cross-talk parasitic current pathways [28]

The main benefit of this cross-talk reducing architecture is that it scales well for large sensors and uses simple analog electronic components which can be easily controlled from a simple microcontroller (Arduino Nano) to make prototyping easier.

The cross-talk reducing matrix driving circuitry selected for this project is similar to that proposed in Sundaram et al. (2019)[34], which uses an improved zero-potential grounding-based readout architecture similar to Figure 10, but the selected row is grounded, while other rows are held at a reference voltage ( $V_{ref} = 2.5 \text{ V}$ ) and the non-inverting input to the op-amp is  $V_{ref}$ , so there are theoretically no parasitic current paths.

### 2.1.1 Circuit Simulation

In order to validate the function of the circuitry and estimate the response behaviour of the sensor a small-scale simulation was created, Figure 11 (interactive Falstad model available at: <a href="https://tinyurl.com/23lt8722">https://tinyurl.com/23lt8722</a>). The Velostat piezoresistive layer is represented as an array of variable resistors connected to columns and rows where the electrodes contact either side. The rows are switched by a number of SPDT (single-pole double-throw) switches that set one row at a time to ground while the rest are set to V<sub>ref</sub>. While a selected row is set to ground, a set of analog switches (representing an analog multiplexer) switch each column individually to the input of a 10-bit ADC (representing the microcontroller).

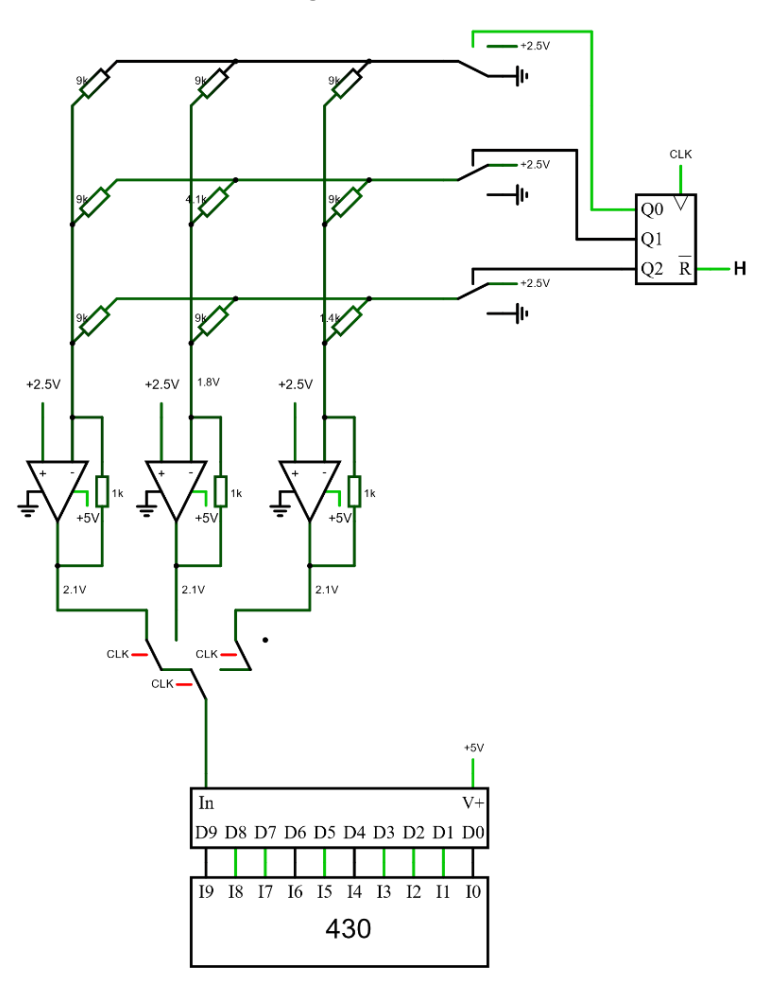


Figure 11 Resistive matrix cross-talk reducing circuitry simulation

Reps (2017)[37], and Sundaram (2019)[34] tested the sensitive range and non-linear response of Velostat. These studies showed that resistance and sensitive range are not largely dependent on the sensor cell size (the overlapping area between perpendicular electrodes). For initial estimations, a 5mm x 5mm sensor size is assumed (25mm²) which gives a predicted sensitive range from 0g ( $\sim$ 10 k $\Omega$ ) to 500g ( $\sim$ 2 k $\Omega$ ) for each sensing cell. Additionally, since the sensor column is connected to the inverting input of the operational amplifiers, the non-linear inverse force-resistance profile from the Velostat is converted to a linear proportional profile, so that applying force to the sensor increases the voltage read by the ADC. The theoretical output voltage ( $V_{out}$ ) of the amplifier is given by [34, 35]:

$$V_{out} = V_{ref} + V_{ref} \left(\frac{R_f}{R_v}\right) \tag{2}$$

Where  $V_{ref}$  = 2.5 V,  $R_f$  is the feedback resistor voltage (1 k $\Omega$ ), and  $R_v$  is the Velostat resistance (2 k $\Omega$  – 10 k $\Omega$ ).

Sliders are used in the simulation to vary resistors within the expected range ( $2 \text{ k}\Omega - 10 \text{k}\Omega$ ) in the matrix to represent applying a force to the pressure sensor. To confirm equation (2), one sensing cell being pressed was simulated by sweeping through the sensitive resistance range and the simulation output plotted (Figure 12). This successfully shows the linear response range from 10 k $\Omega$  to 2 k $\Omega$ , and also captures a predicted saturation of the sensor below 2 k $\Omega$  (equivalent to 0.8 N of normal force applied to a single cell)[34]. This data is useful to estimate required values of the feedback resistors, and also to determine the size of the sensing cells when constructing the full-scale final prototype at a later stage.

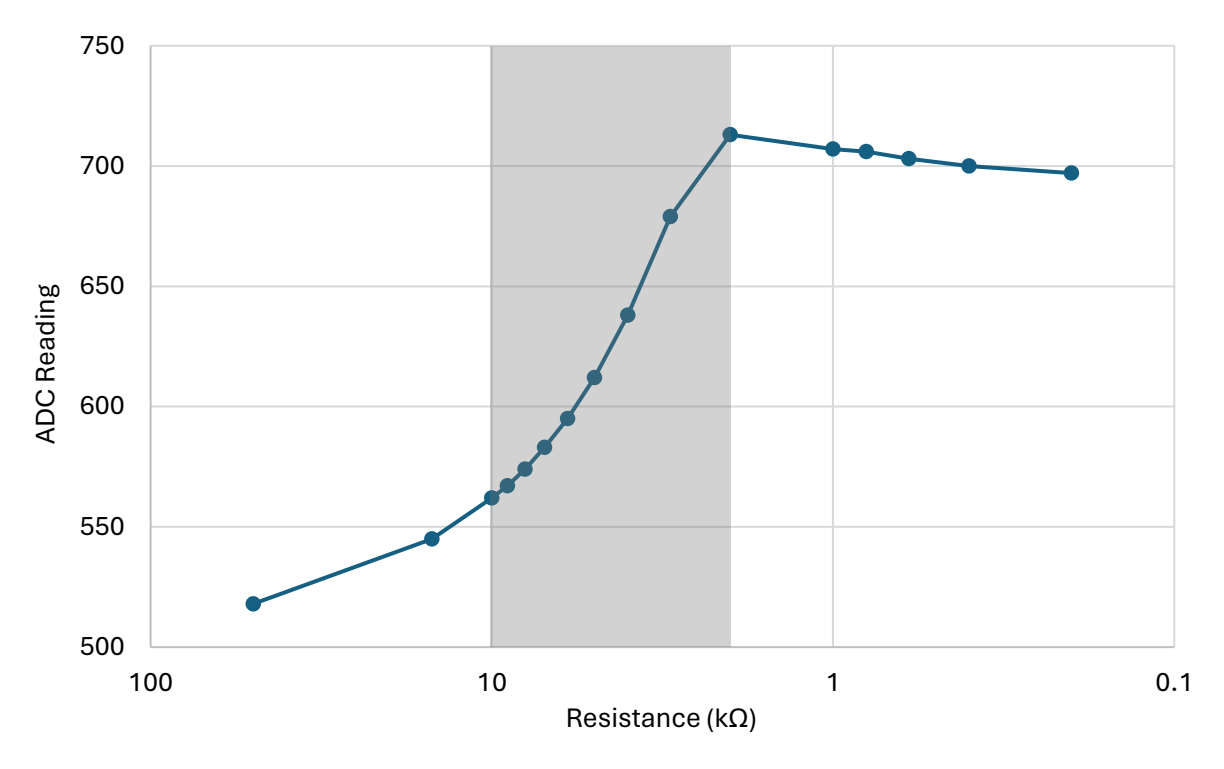


Figure 12 Simulation of ADC readings to show theoretical response to applied pressure to predict sensor output range (highlighted in grey)

## 2.1.2 Breadboard Prototype

For rapid prototyping purposes the cross-talk eliminating circuit was initially implemented on a solderless breadboard. This was done to avoid the lead time of custom PCB manufacture and allowed easy troubleshooting and testing of the circuit. This is based on the same circuit as used in the simulation (Figure 13). The prototype breadboard is shown in Figure 14.

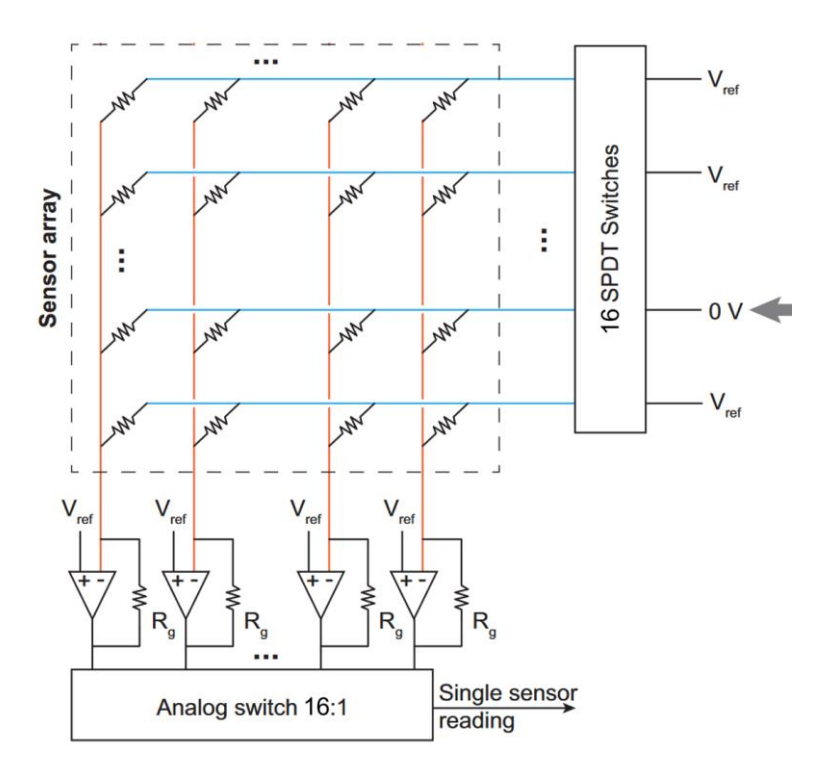
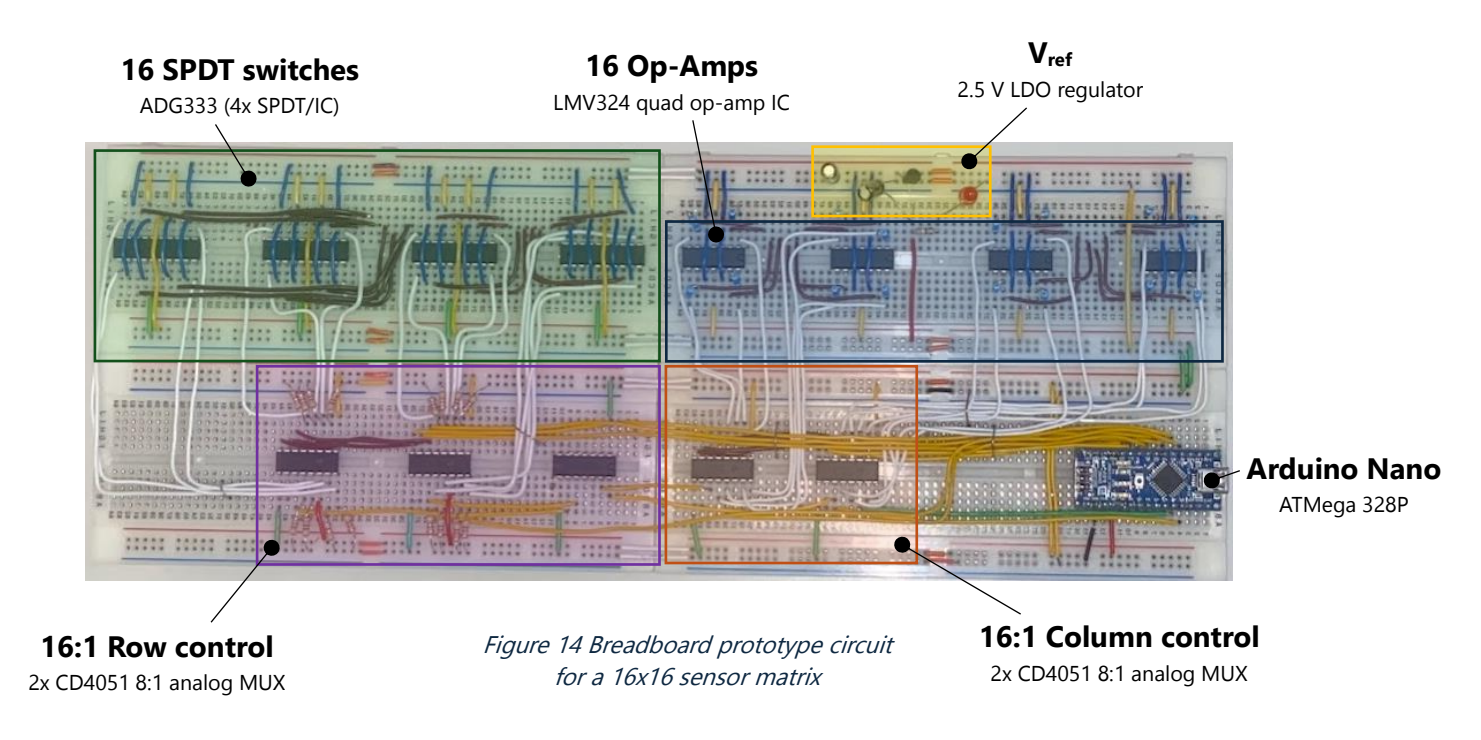


Figure 13 Grounding based isolation readout scheme from Sundaram et al., (2019)[34], adapted for this project



The completed breadboard circuit was tested with a 16 x 16 matrix to confirm the circuit functioned as predicted by the simulations done prior (Section 5.1 covers results of building and testing the 16 x 16 prototype matrix). Ultimately, the breadboard functioned largely as expected except for some faulty ICs. It was not worth troubleshooting the breadboard prototype much since it became clear that the circuitry required to drive larger arrays would be impractical to implement on a breadboard, so it was necessary to move to prototyping a denser double-sided PCB.

#### 2.1.3 Final DAQ PCB

The breadboard prototype demonstrated the circuitry functioned but was unfit for further prototyping as it was bulky, only accommodated a 16 x 16 matrix, and was unreliable due to numerous loose connections which made testing and debugging difficult. Through-hole ICs are also significantly more expensive than surface mount chips, as they are used far less in industry. To drive larger arrays a custom PCB was required. This would still be controlled by an Arduino Nano, with similar analog logic components, but utilising surface mount parts and a double-sided PCB to make the interface board as compact and reliable as possible.

Figure 15 shows a prototype version of the IPRD. The top surface of the inflatable measures approximately 75 x 75 cm. 10 mm/cell is the resolution of most commercially available bed sized sensor, which would total 5625 sensing points for a 75 x 75 matrix. For this project it was not necessary to design a sensor with that resolution or number of sensors, but when designing the final PCB it was practical to accommodate up to  $64 \times 64$  arrays due to electrical components most commonly containing powers of 2 (e.g.: quad op-amp ICs). Since the final prototype for this project had an estimated resolution of 15-30 mm/cell this would create an array of between 25 x 25 - 50 x 50 so there would be extra space on the PCB to accommodate further developments of larger arrays.



Figure 15 Prototype of the IPRD

### 2.1.3.1 Component Selection

Surface mount ICs are cheaper and more widely available than similar through-hole ICs, so these were preferred for the final PCB. Searching for parts was done extensively using parametric search tools on electronic distributors websites (e.g.: Mouser, Digikey, Farnell). The final PCB follows the same schematic as in Figure 13, except for 64 rows and columns instead of 16.

### Reference Voltage:

An external voltage regulator was required to generate the 2.5 V reference voltage used in the sensor matrix. The Arduino can supply a regulated 3.3 V but the internal ADC uses a 5 V reference so this would not leave as much available range for the ADC to measure. Instead an external LDO (low dropout) 2.5 V regulator (TPS76325 - Figure 16)[38] was implemented to provide a steady reference voltage, along with input and output smoothing capacitors and power indicator LEDs. This comes in a compact SOT-23 package.



Figure 16 Texas Instruments TPS76325 2.5 V LDO regulator

### **Analog SPDT Switches:**

A method of switching each row between either ground, or the reference voltage as required next. Single-pole double-throw analog switch ICs were ideal for this application. ICs with 2, 4, 8 and 16 individually controllable switches are available, but there is a trade-off between reducing part count and overall cost, as larger more complex ICs cost more but less are required. As a compromise, the DG333A quad SPDT IC was selected (Figure 17)[39]. These have a switch transition time of <175 ns, giving a theoretical 2 MHz switching frequency, exceeding the kHz frequency of the Arduino ADC by an order of magnitude.

These cost £2.89 each, and 16 of these were required to drive 64 rows giving a total cost of £46. ICs with 2 SPDT switches are available and would have yielded a lower total cost but would double the number required, and came in very small surface mount packages, which would have made building and debugging the PCB more difficult.

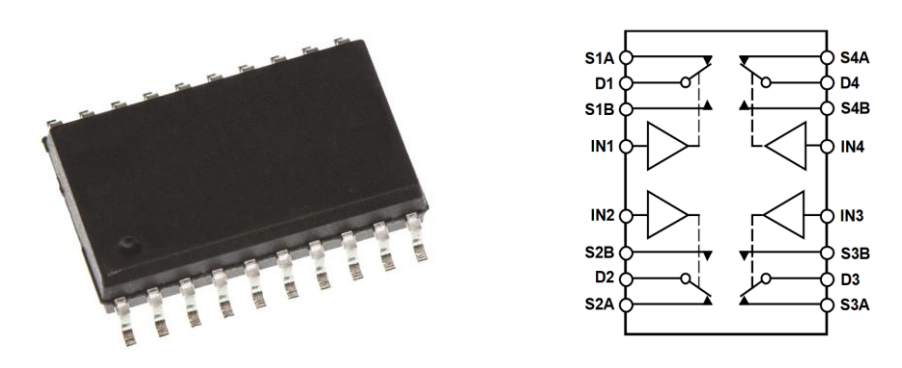


Figure 17 DG333A quad SPDT analog switch IC. Schematic (right) shows all switches with LOW input.[39]

#### 64 Channel Row Demultiplexing:

To control the 64 SPDT switches that send either ground or  $V_{ref}$  to each row, 64 individual control channels are required. The Arduino Nano has 13 Digital Output pins, but through multiplexing only 6 are required to control 64 outputs ( $2^6 = 64$ ). A similar trade-off between size and cost was required since 1:32 and 1:64 multiplexers are expensive but reduce part count, whereas 1:8 multiplexers are cheap but require more parts and space. The 16-channel CD74HC154 were used in this application because they are low cost (£0.53/unit), fast (<220 ns switch time), and come in compact but more prototype friendly SOIC packages [40] (similar to SPDT switches - Figure 17).

Most importantly, these ICs have 2 enable pins on top of the 4 control pins. The 2 extra enable pins effectively give 2-bit control over the 4 individual multiplexers so that the outputs of one is enabled at a time. This is achieved using logic inverter gates (74LVC2G14 [41]) - shown in more detail in Figure 18, pins SW5 and SW6 are the 2 MSB (most significant bits) and are connected to the EN1 and EN2 pins through different combinations of inverted signals through U35 (inverter gate IC). The truth table for the row control is attached in Appendix B.

#### **Operational Amplifiers:**

Each column has one amplifier to process the reading before it is sent to the ADC. The most common ICs come with 1, 2 or 4 amplifiers in compact packages (4 x 4 mm). The LMV324 quad op-amp IC [42] is designed for low voltage (<5 V) operation and offers rail-to-rail output, meaning if it is powered from the Arduino 5 V power they can output all the way up to 5 V, allowing full use of the ADC range. These cost £0.49/unit, totalling £7.80 for the 16 required.

A fixed feedback resistor is also required with each amplifier. The size of this was selected as  $1 \text{ k}\Omega$  during the simulations detailed previously. As a rule of thumb this value should be close to the expected resistance of the velostat when pressed, and around 10x lower than the open-loop resistance [35]. Small surface-mount resistors are negligible in cost (0.01/unit).

#### 64 Channel Column Multiplexing:

The output of each amplifier must be connected to an Analog Input of the microcontroller. The Arduino Nano only has 8 inputs, so multiplexing is again required. The 32:1 ADG732 multiplexer [43] was selected for this as it allowed a more compact solution than using more multiplexers with fewer channels. It also has excellent ON-resistance ( $<4~\Omega$ ) compared to cheaper options, which is important to maintain signal quality. Table 7 compares 2 widely available cheap multiplexers (CD4051 and CD4067) to 2 more expensive modern multiplexers which could be used in this application.

Since every column is sampled for each row, the chosen multiplexer has to switch 64x faster than the row controlling multiplexer. The need to maintain the sensor voltage and the one-off nature of the prototype means that it is worth using more premium parts to ensure solid function.

Table 7 Comparison of multiplexer options for switching columns to Arduino Analog Inputs. Prices from Mouser[29], data from relevant data sheets.

Multiplexer	Channels	Cost/unit	ON resistance	Switching time
ADG732	1:32	£8.11	4 Ω	23 ns
ADG1606	1:16	£8.32	4.5 Ω	175 ns
CD74HC4067	1:16	£0.54	70 Ω	60 ns
CD4051	1:8	£0.34	470 Ω	450 ns

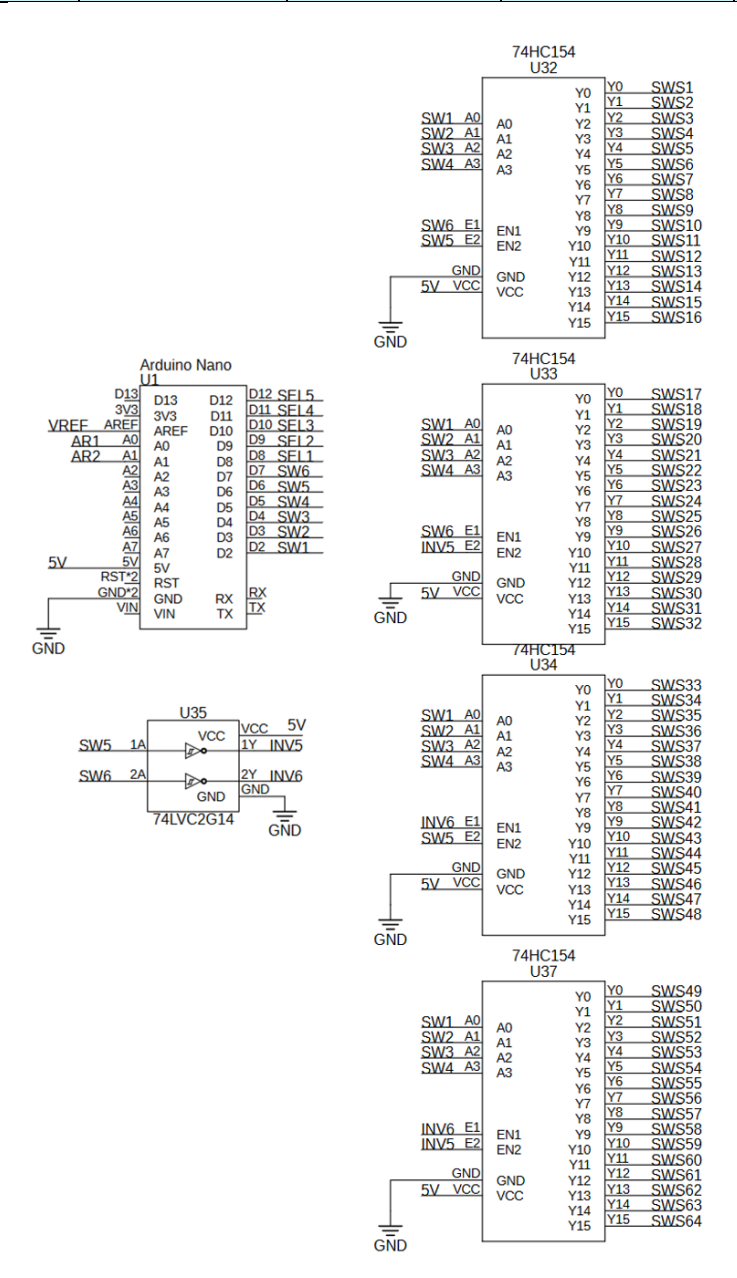


Figure 18 Section of the full PCB schematic showing the Row control logic. 6 Arduino Digital Output Pins: D2 to D7, send a low signal to one row at a time in order

## 2.1.3.2 PCB Design

Figure 18 shows part of the final PCB schematic relating to the row control multiplexers. The full schematic is available in Appendix A. After completing the schematic, the next stage of designing the PCB is creating a PCB layout. This involves setting the component locations, routing traces, and placing vias. There are many rules-of-thumb and general guidelines which should be adhered to while designing PCBs (see [44]). For example, placing connected components near each other to minimise trace length (and associated noise/voltage drops), minimising board size where possible to save cost, and also accessibility to parts for debugging and testing are especially important for PCB prototyping.

The complete PCB layout is also shown in Appendix A. This could be made more compact by further optimising placement of components, and sourcing components with smaller footprints, but for the purposes of this project this PCB was adequate for demonstrating functionality.

The final design is a double sided 170 x 100 mm PCB. For this project, the most cost effective manufacturing option was external manufacturers (e.g.: JLCPCB or PCBway [45,46]). 5 blank pressure sensor driving PCBs cost £35 (£7/board) with a lead time of 1 week. Figure 19 shows both the PCB layout and manufactured PCB side-by-side and Figure 20 and Figure 21 show the complete PCB with sections highlighted by function similar to Figure 14.

The complete PCB was used with the full-size prototype to confirm functionality of the whole system (see Section 5.2).

All PCB design and manufacturing files are available in the Supporting Documents folder.

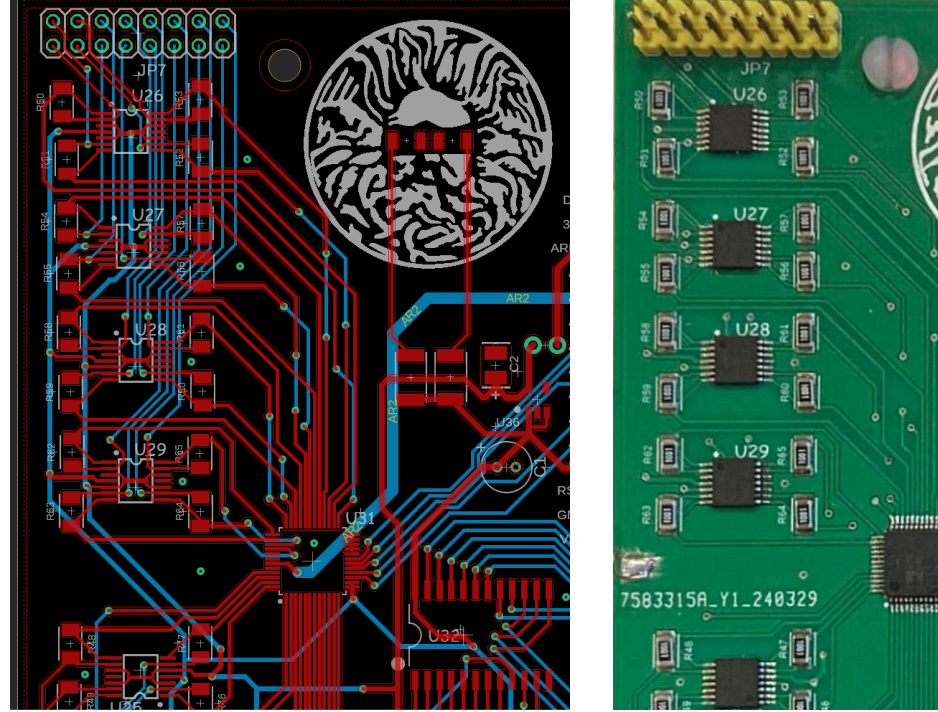


Figure 19 PCB layout (left), compared to manufactured and built-up PCB (right)

## **Row control logic**

64 channels

Figure 20 Final built-up prototype PCB, with functional sections highlighted

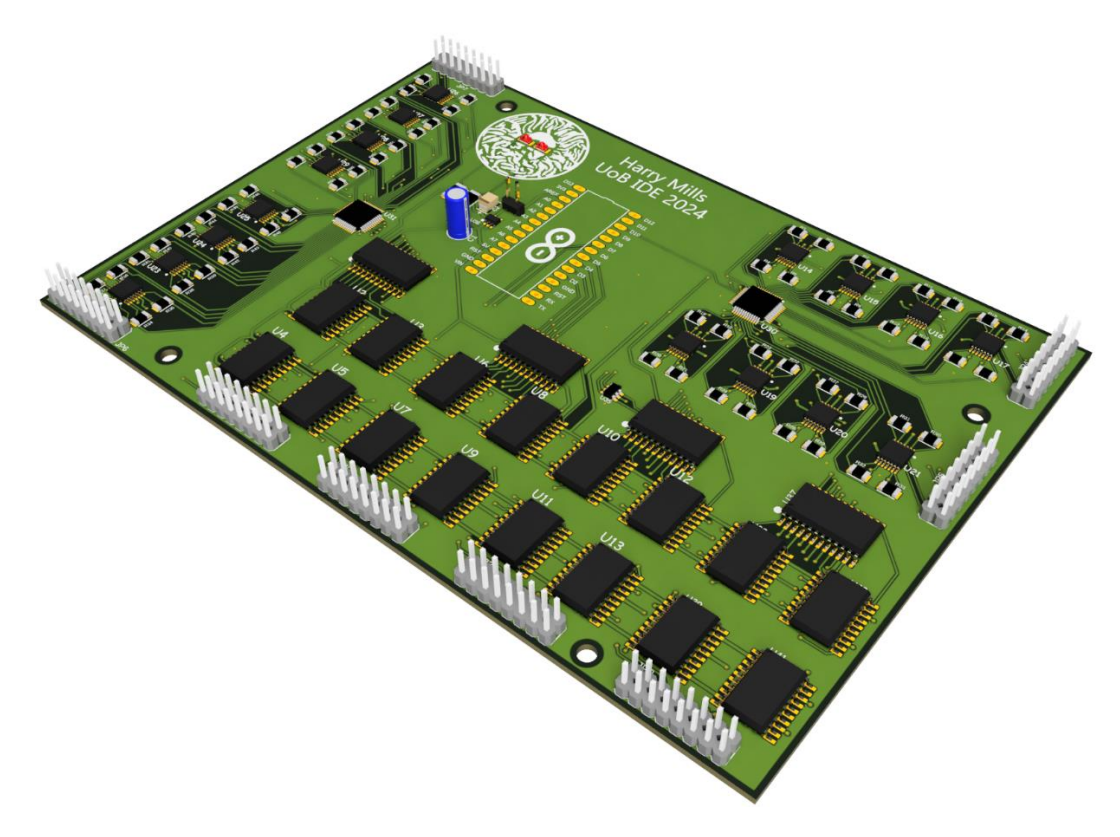


Figure 21 Prototype PCB CAD model

# 3 Software Development

The initial proof of concept prototype was driven by an Arduino script that controlled the rows and columns, sending voltage readings over the serial monitor to a Processing script for visualisation (see Figure 5-Figure 6). This functioned successfully for the small sensor, but larger arrays required optimisation to maintain refresh rates >1 Hz, and more a complex GUI (Graphical User Interface) was desired to give the user more information. The software also had to be modified to run the specific components selected for the PCB detailed above.

Complete code for driving the pressure sensor matrix and visual processing is attached in the Supporting Documents folder.

### 3.1 Arduino Code

Figure 22 shows the flowchart of the final Arduino code for driving the pressure sensor matrix. The setup section compromises of initialisation commands to set the logic control pins and begin communication with the user interface visualisation. The main section of the code loops through all rows and columns to scan the entire matrix. The process of this is firstly setting a selected Row to ground via the SelectRow(X) function. Then, while that row is set to ground, taking a voltage reading of each column in turn. To reduce noise in the data multiple readings are taken at each column and averaged before being sent to the visualisation code. Once every column has been measured, the code loops on to the next row, where all columns are again measured. After every column has been measured for every selected row the Arduino sends a '0' to the visualisation code to indicate the end of a frame, and the code loops again from the first row.

## 3.1.1 Optimisations

Mini-Study 2 identified the *AnalogRead()* command as a key bottleneck in the Arduino software driving the pressure sensor. By default, this takes 13 clock pulses of the 125 kHz ADC clock (100  $\mu$ s). This can be increased by modifying the pre-scale of the ADC clock speed [47]. This can be increased up to 1 MHz before becoming excessively noisy, meaning that *AnalogRead()* takes 17  $\mu$ s (76 kHz) and a 150 x 100 array can theoretically be scanned at 5 Hz, 8 times faster than the default speed. This can be achieved with low-level code run when setting up the Arduino, detailed in Appendix C.

Another bottleneck in the original approach was observed when setting the row and column pins controlling the multiplexers. Originally this was achieved by individually setting each pin consecutively using the digitalWrite() function. However, the scanning rate was doubled using Port Manipulation [48]. This allows pre-specified sets of microcontroller pins to be set to HIGH or LOW simultaneously. For example, setting PORTD = 52, simultaneously converts 52 into binary (00110100) and sets pins the 8 pins in Port D (D0–D7) based on these values. This was facilitated in the final PCB by connecting the row and column logic controls to separate ports (Figure 23).

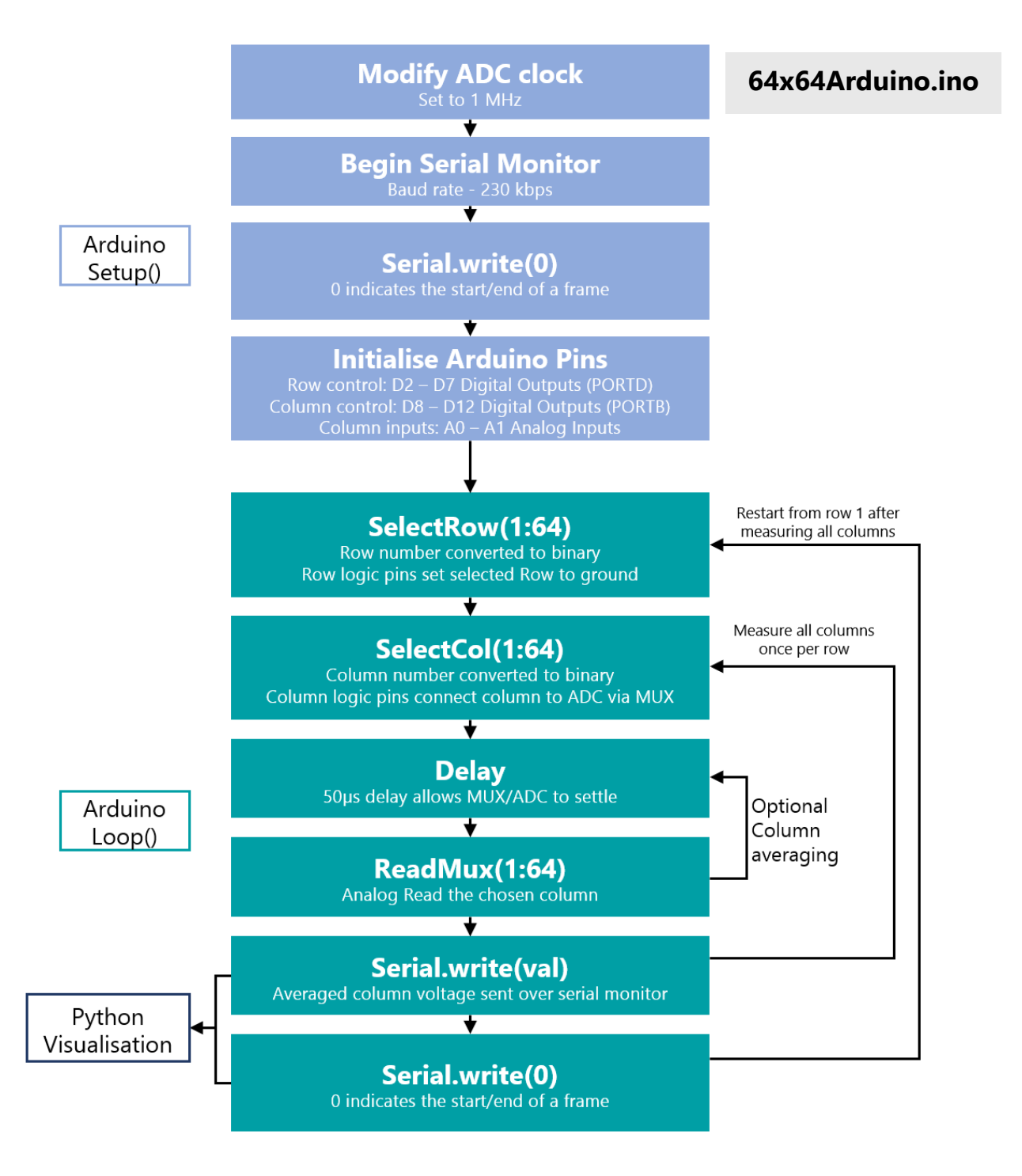


Figure 22 Final Arduino Code Flowchart (64x64Arduino.ino)

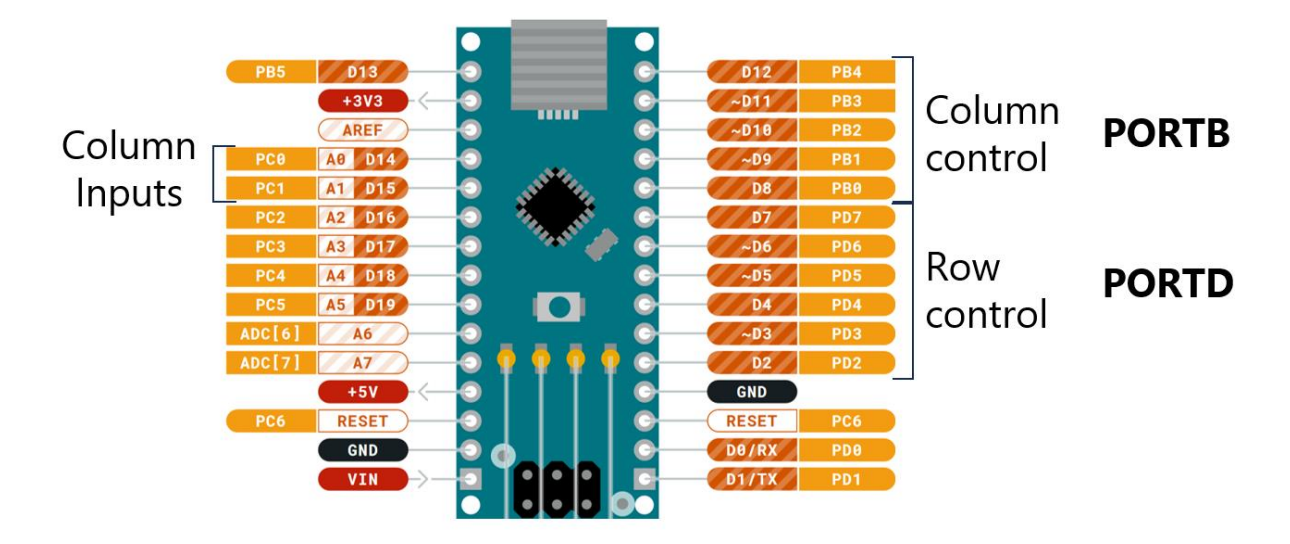


Figure 23 Arduino Nano pinout highlights row and column logic is aligned with AVR microcontroller ports to allow simultaneous setting of pin states.

Another option for increasing sample rate is to use an external ADC. External ADCs controlled over serial communication can have sample rates of over 500 ksps (kilosamples/second), at 16-bit resolution (Figure 24 [49]). However, for the purpose of this project, the previously implemented software optimisations were adequate to drive the sensor at ~1.5 Hz and added hardware complexity was deemed unnecessary. Ultimately, increasing scanning speed is not very important within the context of this project as pressure sores form over hours from persistent pressure points, but faster sampling does allow more readings to be taken for an average (innermost loop Figure 22) within the same time period, reducing noise in the data.

The final identified bottleneck in the prototype is the serial communication between the Arduino Nano and the visual processing script in Python. The baud rate (data transfer rate) is set to 230 kbps (kilobits/second), or 28 kBps. Increasing the baud rate much beyond this is unreliable. A 64x64 sensor has 4096 sensing points. If an 8-bit ADC resolution is used to measure each cell, this generates 4096 bytes per scan. This sets a hard limit of 7 Hz scanning, which would be even lower if 10 or even 16-Bit ADC values were used. Improving this requires high-level architectural changes to the sensor driving circuitry such as using a USB interface or a more sophisticated microcontroller. This is discussed further in the future improvements section but was deemed out of scope for this project.



Figure 24 External ADC, 500ksps, 16-Bit resolution

### 3.2 Visualisation Code

The visual processing and graphic user interface (GUI) were written in Python for the final prototype, as this was more familiar and facilitated adding buttons to control to the live-updating pressure map.

Figure 25 shows the flowchart of this code. The relevant interfaces between the Arduino Code and Python visualisation code in Figure 22 are the *Serial.write()* commands which send the column readings, and signals to indicate the start/end of each frame.

The code begins by importing the relevant libraries, initialising the serial communication, and then running a calibration. This must be done with no weight placed on the mat as it takes 5 consecutive frames, averages the values, and applies this as a constant offset on incoming data.

Next, the code waits until a '0' is sent over the serial monitor, this indicates the start of a new frame. When a '0' is read, the code enters a loop which reads a byte for every sensing cell in the array and stores it in a matrix of similar size to sensor array. Once every sensor point has been measured the full matrix represents one frame of pressure sensor data. Interpolation can be performed here to smooth the data, as well as finding average and peak pressures for the top, middle and bottom thirds of the sensor. The average and peak pressure values are used to control the pneumatics in an optional 'pressure relief mode' (see Section 4). Finally, the complete pressure sensor frame is plotted on the display.

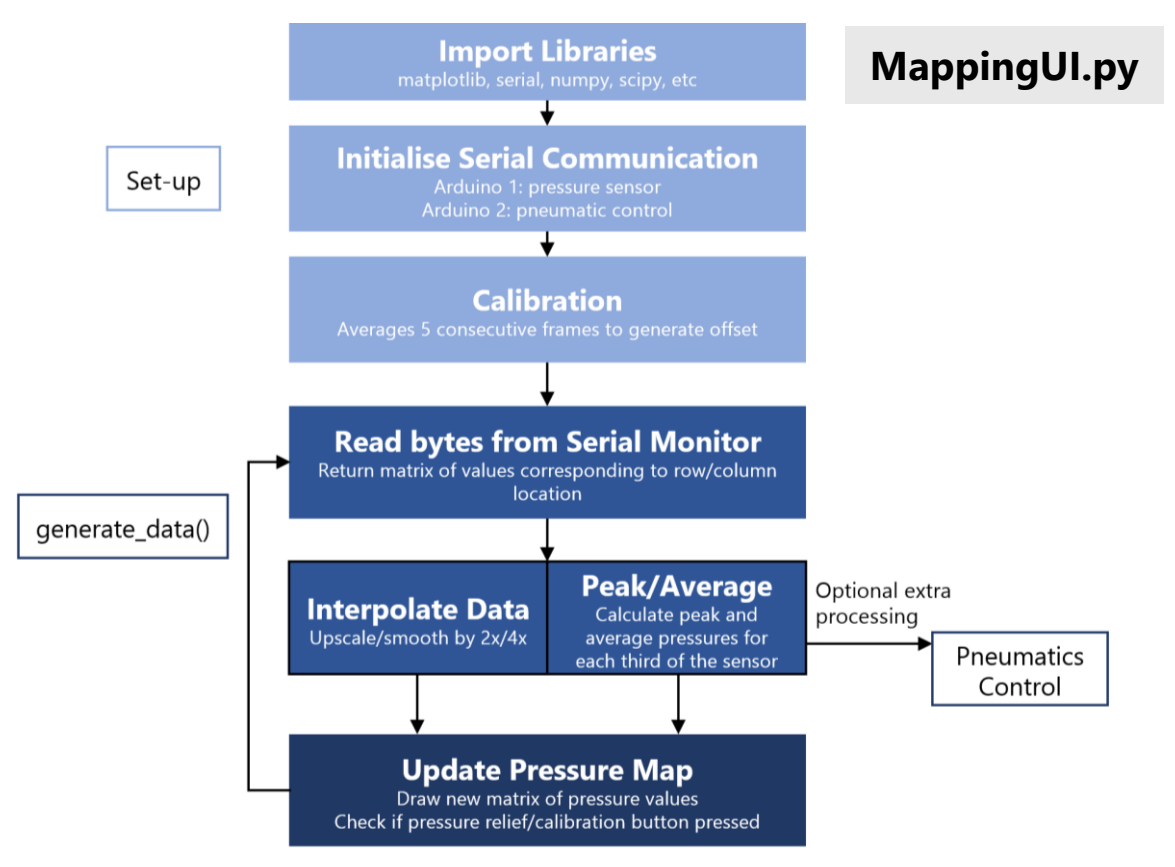


Figure 25 Python Visualisation and User Interface high-level flowchart (MappingUI.py)

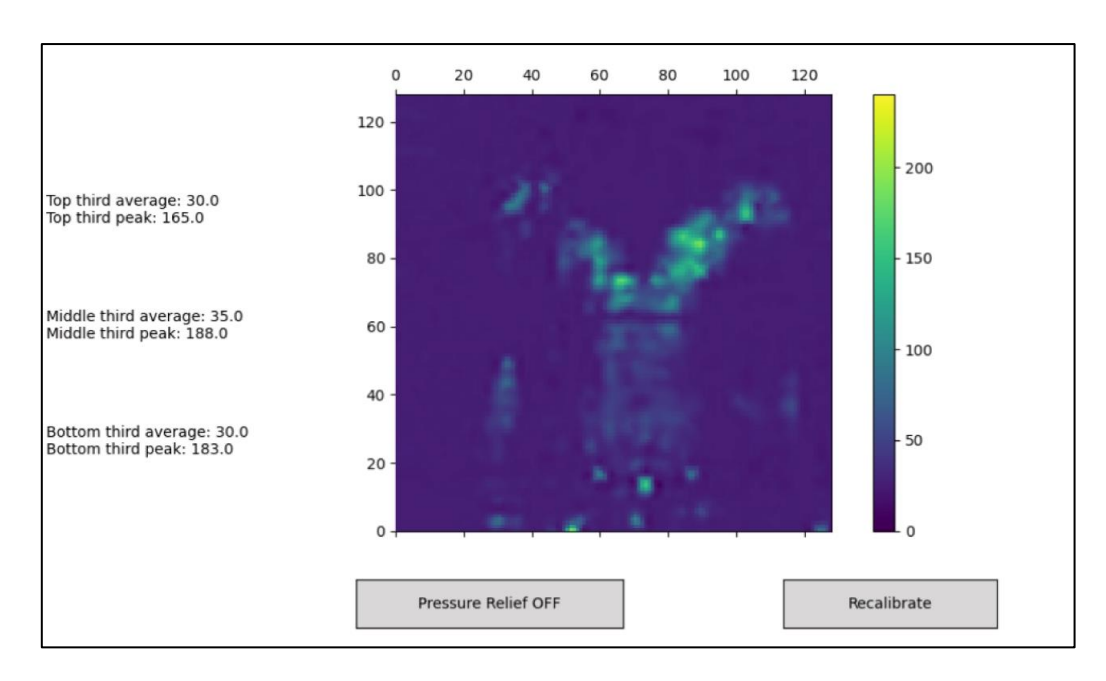


Figure 26 Screen capture of the live pressure map showing peak and average pressures for each third, and buttons to toggle pressure relief mode, and recalibration

Figure 26 shows a screen capture of the final user interface generated by the MappingUI.py script. This includes a recalibration button which aggregates 5 consecutive frames to create a new constant offset, and a pressure relief toggle button which initiates a control of the pneumatics via a second Arduino connected to the processing PC. Pneumatic control code is detailed in the next section.

The colour scale ranges from 0-255 (8-bit). This was convenient to allow data for each cell to be sent in 1 single byte over serial, rather than 2 separate bytes which would give more pressure resolution levels, but half the refresh rate. However, the internal Arduino ADC takes 10-bit readings. From previous circuit simulations (Section 2.1.1), only a range of voltage can theoretically be outputted from the amplifier of each row, 2.5 – 5 V, which correspond to a usable range of 512-1024 (10-bit). However, in practice, the usable range is 512-950, as any values above 950 can only occur from shorted electrodes since Velostat resistance levels off as more force is applied [34]. This still leaves over 400 so some resolution is lost when mapping the values to 8-bit resolution in the Arduino code, but the refresh rate is twice as fast as sending 2 bytes per cell. Figure 27 details this mapping.

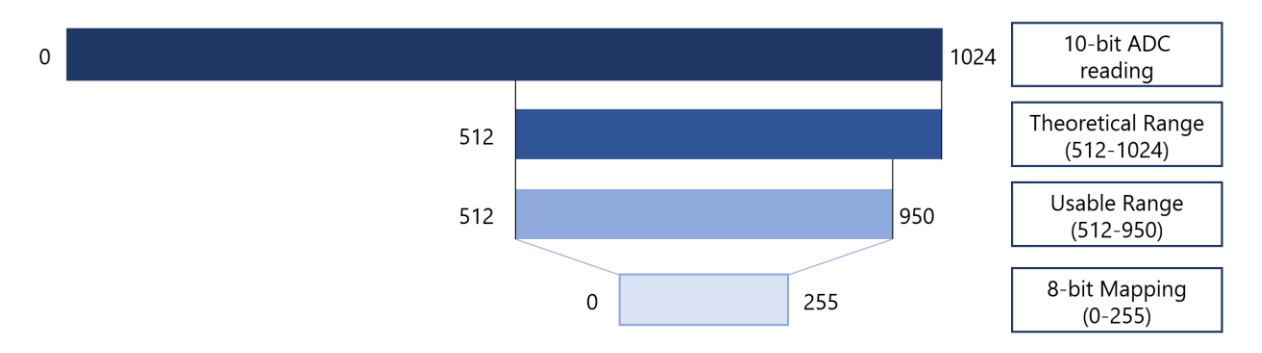


Figure 27 Mapping scheme to send 10-bit ADC reading in 1 byte based on circuit architecture constraints

# 4 Pneumatics Development

Developing the pneumatics to control the IPRD vessel was not the main focus of this project, but it was within the scope to develop a feedback system using the pressure sensor data to control the inflatable in real-time. This required additional software to interface with the Arduino controlling the pneumatic valves, and development of baseline pneumatic controls to inflate each chamber of the IPRD in the desired fashion.

### 4.1 Pneumatic Hardware

Inflatable vessel design and pneumatic control of the IPRD was the focus of previous projects (Luke Ortlieb, Anders Vangsgaard (2022-2023) [50,51]), so further pneumatic control developments are left to the future improvements section of this project. Additionally, parallel to this project, Anders Vangsgaard was developing a final IPRD prototype to enter medical trials. For this project it was necessary to develop baseline pneumatic control to drive the new 3-chamber inflatable to demonstrate that the pressure sensor could be integrated with the inflatable.

As mentioned, previous work was expanded for this, using similar relay-driven solenoid valves as Luke Ortlieb's project (2023), modified for control of a 3-chamber vessel and simplified by removing air pressure sensor feedback (which proved unreliable), and the push-button physical interface (Figure 28). The pneumatic schematic for this is presented in Figure 29. The uses a set of 2/2 (open/closed) solenoid valves to control the opening of each inflatable chamber individually. A 5/2 valve switches between applying pressure to the chamber openings (Low state), or a vacuum (High state) which is created by the Venturi vacuum generator. In this configuration the inflatable chambers can be in 3 states: inflating, deflating, or closed.

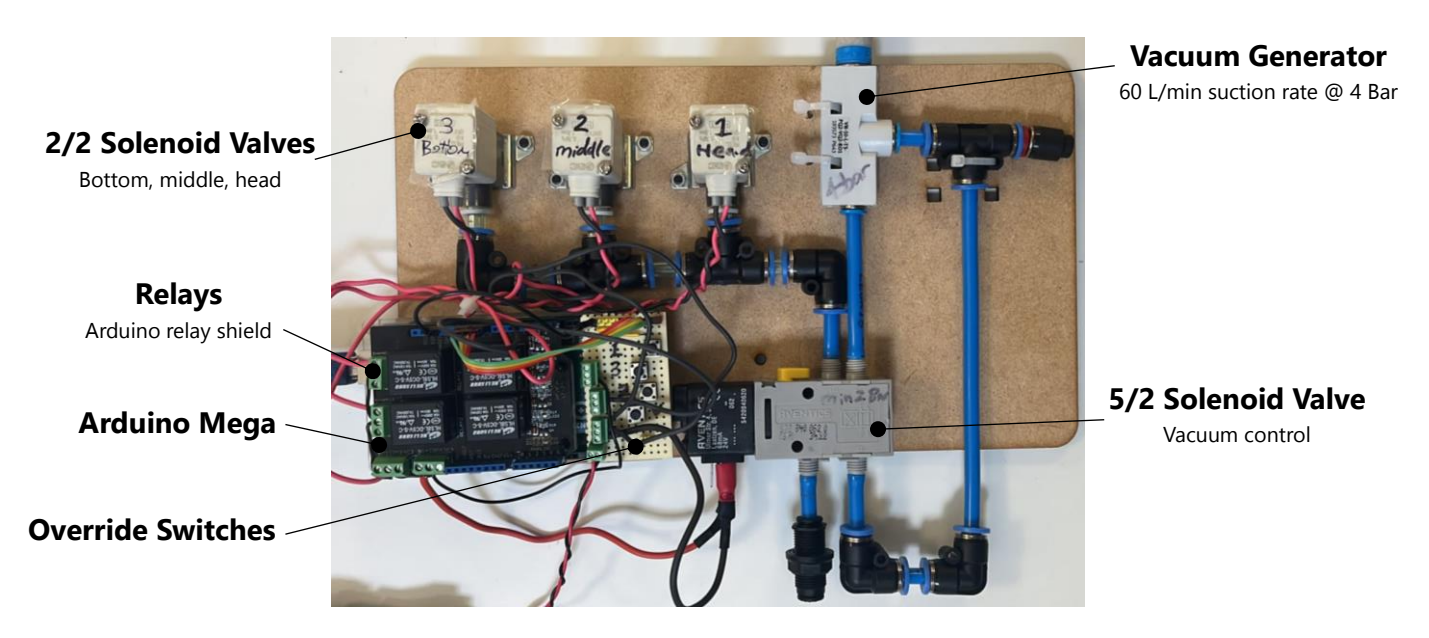


Figure 28 Pneumatic hardware to control the IPRD prototype. Pneumatic schematic presented in Figure 29.

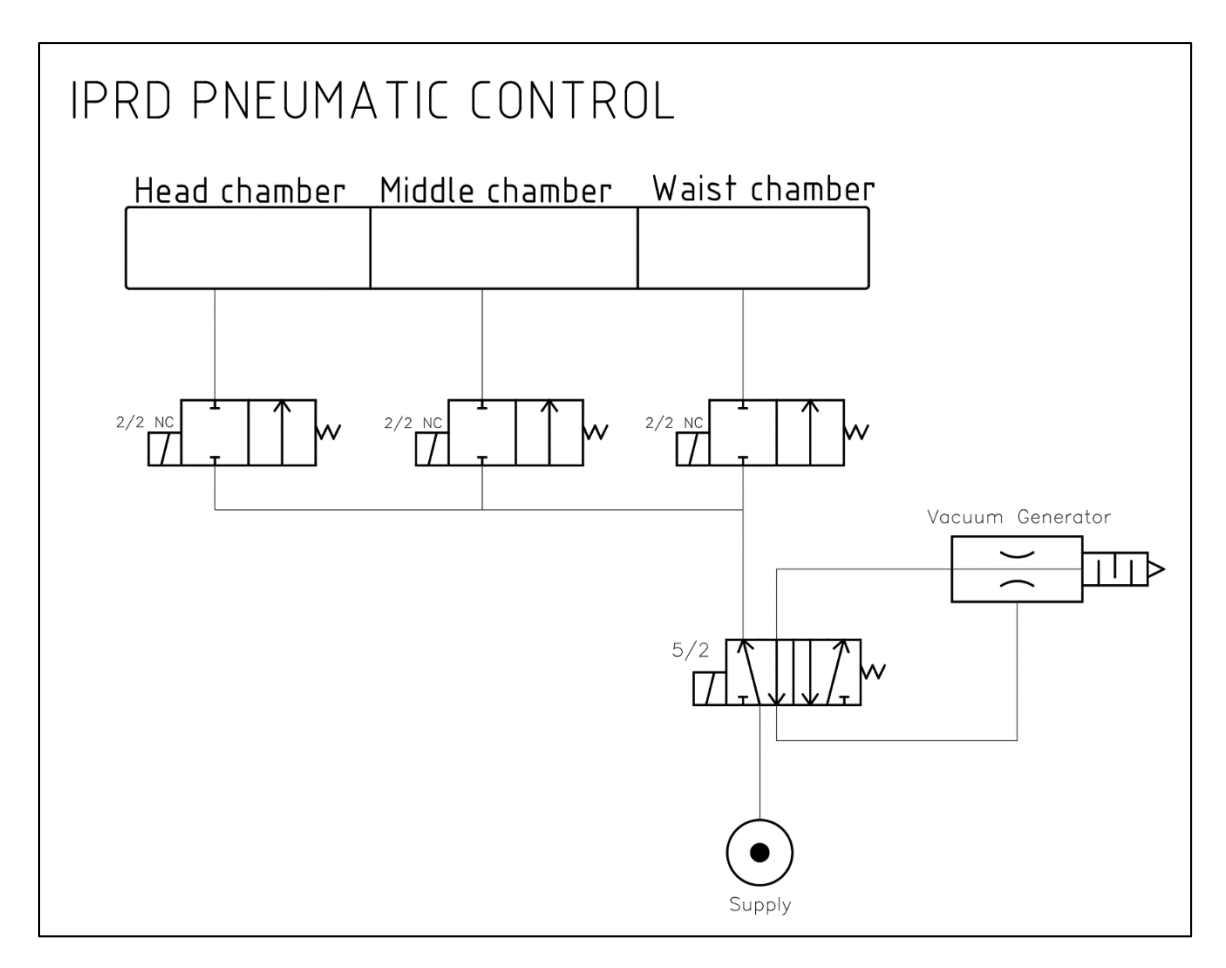


Figure 29 Simplified IPRD prototype pneumatic schematic

### 4.2 Pneumatic Software

To enable automatic control of the inflatable using pressure sensor data, the pneumatic valves were controlled from a microcontroller connected to the same PC used for processing the pressure mat data (Figure 9). The pneumatics logic was controlled by an Arduino Mega, with the solenoid valves powered by an external 24 V power supply switched by relays controlled by the Arduino.

This work was completed towards the end of the project timeframe, so there was only time to demonstrate the proof-of-principle that pressure sensor data could be used to inflate the IPRD in closed-loop control. There was no opportunity to run user tests with doctors/nurses to gain insight on the expected behaviour of an automatic repositioning system. However, as discussed in the future improvements section, there is scope for more sophisticated control algorithms that can reposition more effectively and use the pressure sensor data to a greater extent.

Override buttons were also implemented as a method to inflate the IPRD without using the automatic feedback.

For the purposes of this project, as a demonstration, the control flowchart is given in Figure 30. Every 20 seconds, the visualisation processing code samples the latest pressure data frame by sending the peak and average pressures for the top, middle and bottom third over the serial monitor to the pneumatic controller Arduino. These values are then compared to a threshold, and pneumatic valves are opened for 5 seconds to inflate sections of the inflatable where the corresponding pressure sensor section is over the threshold average or peak pressure. The code then waits until more peak and average pressures are sent from the PC. If the next check indicates that pressure in any previously inflated sections is now below the threshold these sections are vacuumed for 10 seconds to deflate them. If any sections have pressures over the threshold in consecutive checks, these chambers are left closed to avoid overinflating the IPRD.

The pneumatic control code is attached in the Supporting Documents folder.

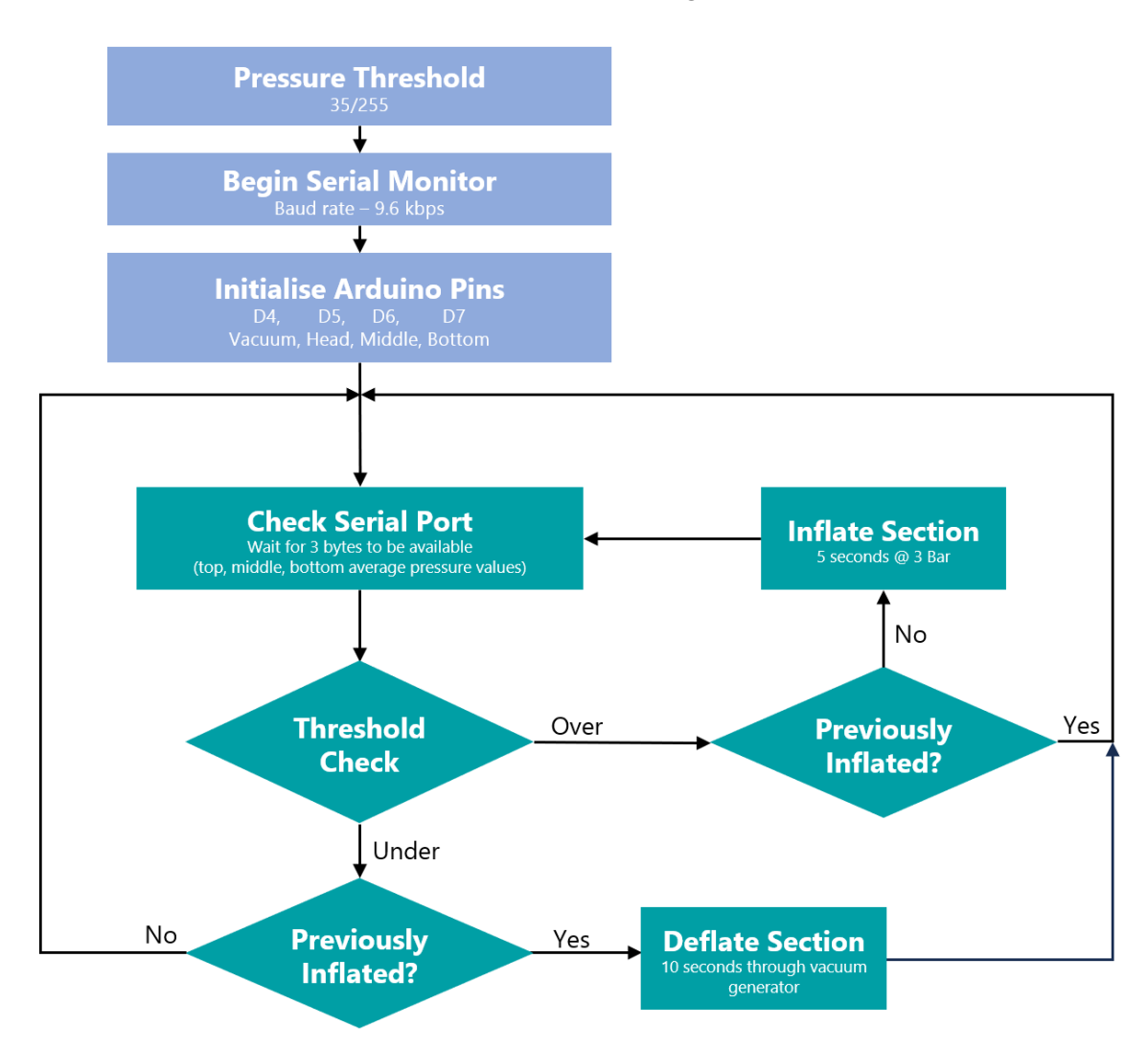


Figure 30 Flowchart of pneumatic control software to demonstrate pressure sensor data can be used to automatically control the inflatable

# 5 Electrode Development

The final development area of this project highlighted in the original system diagram (Figure 9) is the electrodes. To build a matrix of sensors, many parallel rows of thin, flexible conductors were required. For initial small prototypes (7 x 7 and 16 x 16) copper tape was used as a cheap prototyping material. Ultimately, copper tape was also used for the full-size prototype, but work was also done to design a screen-printed alternative using conductive ink on polymer substrates as a more professional option that could be more easily manufactured in larger quantities in the future.

The piezoresistive layer was not focused on in this project as Velostat was deemed suitable for prototyping needs. Piezoresistive alternatives that could be considered in the future and detailed in the future improvements section, as well as alternative electrode constructions.

## 5.1 Initial Prototype Mat

Figure 31 shows the 16 x 16 small-scale ( $20 \times 20 \text{ cm}$ ) prototype used for testing the breadboard electronics. This used copper tape traces on a plastic film with velostat sandwiched in between. Copper tape was a good choice for this as it is thin, flexible, highly conductive, cheap, and has adhesive backing.

This prototype had a resolution of 12 mm/cell by using 6 mm wide tape with 6 mm spacers. This was more than sufficient to identify individual fingers of hands and shapes of objects placed on the mat.



Figure 31 16 x 16 prototype sensor

Key problems with this prototype included making wired connections. Connecting to the matrix interface electronics requires a wired connection. This is a key benefit of using copper tape over conductive textile electrodes since copper can easily be soldered to. However, the plastic film substrate was not heat resistant and the connections had to be reinforced to protect the solder joints.

Another problem was the limitation of using off-the-shelf copper tape. This limited the trace width to 6 or 12 mm, and therefore the size of the sensing cells. Secondly, laying all traces by hand was very labour intensive since the tracks had to lie flat, straight, and parallel. Since the tape was only 0.04 mm thick it was also liable to breaking while being placed.

A final problem was that the layers of mat were difficult to keep aligned. Since the plastic film the electrodes were placed on was not adhesive itself it could move relative to the Velostat and the opposite layer of electrodes. This was mitigated by adding tape around the edge of the sensor, but the layers could still separate and did not perform well on non-flat surfaces.

# 5.2 Full-size Prototype

Screen-printing electrodes for a full-size prototype was not possible within the timeframe of the project. The final full-scale prototype was constructed similarly to the previous iterations. To cover the surface of the IPRD (Figure 15) it had to measure at least 70 x 70 cm. Caggiari et al., (2023)[15], demonstrated that sampling down to 7.5 cm/cell was sufficient for detection of posture and mobility events (Figure 32). This would only require a 10 x 10 matrix. However, increasing the resolution means that pressure points can be located more accurately, and the sensor is more versatile since other projects requiring more spatial resolution can use the same sensor (e.g.: if the IPRD were redesigned to have more separate chambers higher spatial resolution allows better automatic repositioning).

A target of 12 mm/cell is practical since copper tape is widely available in 6 mm width rolls. A track can be placed, and its adhesive cover laid next immediately next to it to create a parallel 6 mm gap for a total of 12 mm between each electrode. To cover the IPRD, this resolution requires a 58 x 58 array of electrodes.

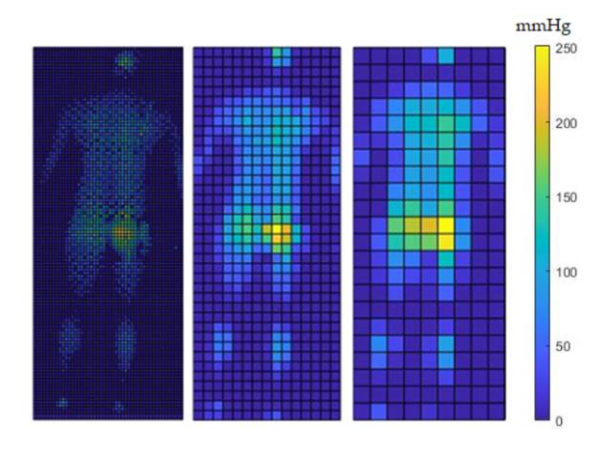


Figure 32 Image from Caggiari et al., (2023)[15] demonstrating down-sampled pressure sensor data can still effectively detect posture and peak pressures

A changed based on previous prototypes was to use a substrate that was more durable than the plastic film used in the small prototype, while still being waterproof. Vinyl sheet used for car wrapping[52] was ideal for this as it is strong, waterproof, and has adhesive backing meaning that layers would not move relative to each other once the sensor was built.

Building the final full-size sensor was quite labour intensive so this method of constructing a pressure sensor should only be considered for one-off prototypes. Figure 33 shows one set of electrodes part-completed. A total of 70 m of copper tape had to be cut into 100 x 70 cm sections, and then painstakingly laid down on the adhesive vinyl substrate. Attempting to lift and replace copper tracks often resulted in them snapping and the whole row would require replacing. After placing a trace, the sticky-back cover was placed adjacent. This was repeated for the entire width of the 70 cm sheet. Ultimately, due to stacking errors when placing tape and spacers the resolution averaged to 14 mm/cell, which meant that only 50 rows could fit on a 70 cm sheet. Due to the design of the PCB and ease of making connections a multiple of 16 was desirable, so the final sensor was trimmed to a **48 x 48 array** over **68 x 68 cm**. The final full-size sensor mat is shown in Figure 34.

The main problem encountered when constructing the full-size prototype was assembling the layers once all copper tape had been placed. To do this, the spacers were removed to expose the vinyl substrate adhesive, then sheets of velostat were placed down. Care was taken to place these as flat as possible without leaving any copper exposed which could cause shorting between layers. Then the two halves of the sensor had to sandwiched together. This had to be done carefully due to the adhesive of the vinyl making it almost impossible to unassembled and reposition the layers once they had been stuck together. Some ridges can be seen in Figure 34 where layers did not go perfectly flat. This was tolerated as fixing it would likely cause damage to the sensor mat when taking the layers apart, and it would likely not cause many problems in the data.



Figure 33 Assembly process for one side of the pressure sensor mat

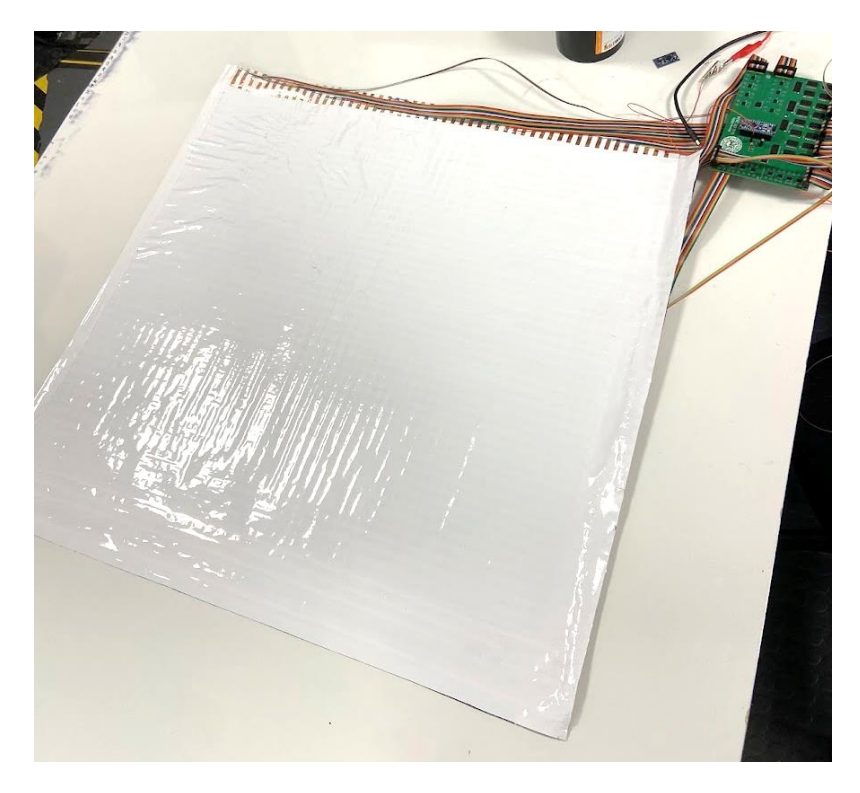


Figure 34 Completed full-size prototype pressure sensor array

## 5.3 Screen Printed Design

Screen printed electrode designs were also produced for this project. Screen printing conductive silver ink on a polymer film is the most common way of creating the rows and columns of electrodes in commercial pressure sensors. Large sheets of electrodes can be quickly and cheaply manufactured once the tooling is created, requiring only a small amount of conductive silver ink. Figure 35 shows a diagram of a typical roll-roll screen printing process and a typical example of a screen-printed pressure sensor matrix.

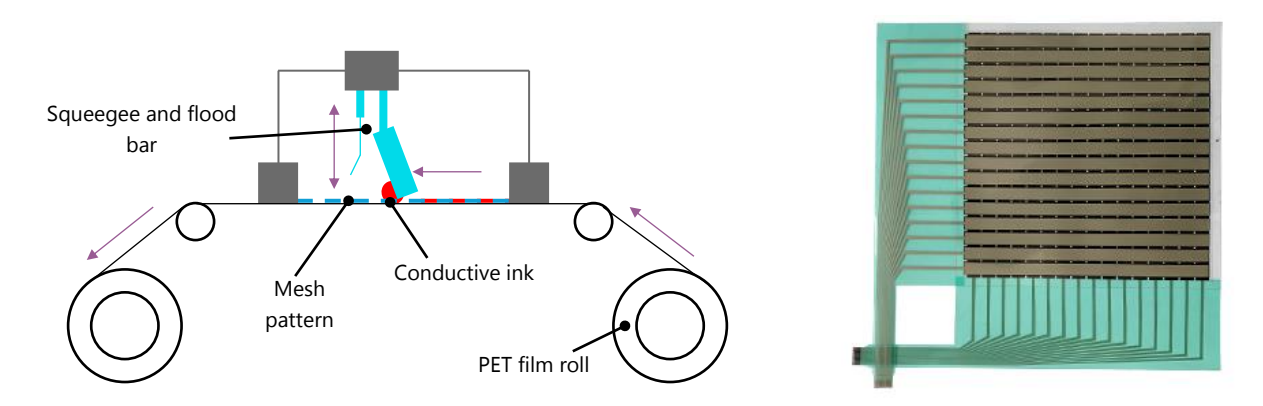


Figure 35 Left: Simplified diagram of a roll-to-roll screen printing process.

Right: Example of a screen-printed resistive pressure sensor

The University of Bath has a small screen-printing rig (accommodating 200 x 300 mm sheets). Two iterations of screen-printed electrode sheets were produced; schematics are available in Appendix D. Improvements between iterations include:

- Removing sharp angles: Due to the flexible substrates, cracks will propagate from corners in the design. Sensing pads and traces were redesigned.
- Interface connector: All electrodes can be connected to an Amphenol Clincher [53], designed for making compact connection to flexible circuits. This was required since screen-printing substrates are not heat resistant enough to be soldered to.
- 16 x 20 resolution: 10 mm/cell was designed to match commercially available sensors

The process of producing the tooling for screen printing has multiple steps. Information for using the screen printing rig at the University are attached in the Supporting Documents folder [54]. To summarise:

- Design the electrode pattern in vector graphics software (AutoCAD, Inkscape, Illustrator)
- Print this pattern on a transparency film as a **positive** Figure 36 (i.e.: ink is deposited where the electrode should be)
- Apply photosensitive emulsion to the screen. This must be left to dry away from bright light sources for 24 hours.
- Expose the photosensitive layer with UV light with the printed positive electrode pattern on top. This cures areas of the photoresist that are not covered by the ink.
- Wash the exposed screen. Using a jet washer wash the screen to remove emulsion where there was no photoresist covering.
- Place the finished stencil in the printing rig and scrape through a layer of conductive silver ink on to the substrate placed below. The electrode sheet then must be dried at 120°C for 30 minutes.



Figure 36 Example of a positive transparency used as a photoresist when exposing

#### 5.3.1 Problems

Ultimately, it was not possible to produce any screen-printed prototype electrodes for this project due to time and budget constraints.

Due to the small rig available at the University, to produce the full-size prototype, tessellating many small screen-printed sheets was required (Figure 37Figure 35) by sticking them together. One problem with this was the increased number of connections to the sensor. Making electrical connections between sheets was difficult without introducing rigid components (wires and solder) into the sensor structure, a row of connections would be required along the top and bottom of the mat, doubling the number of connections to the interface PCB required.

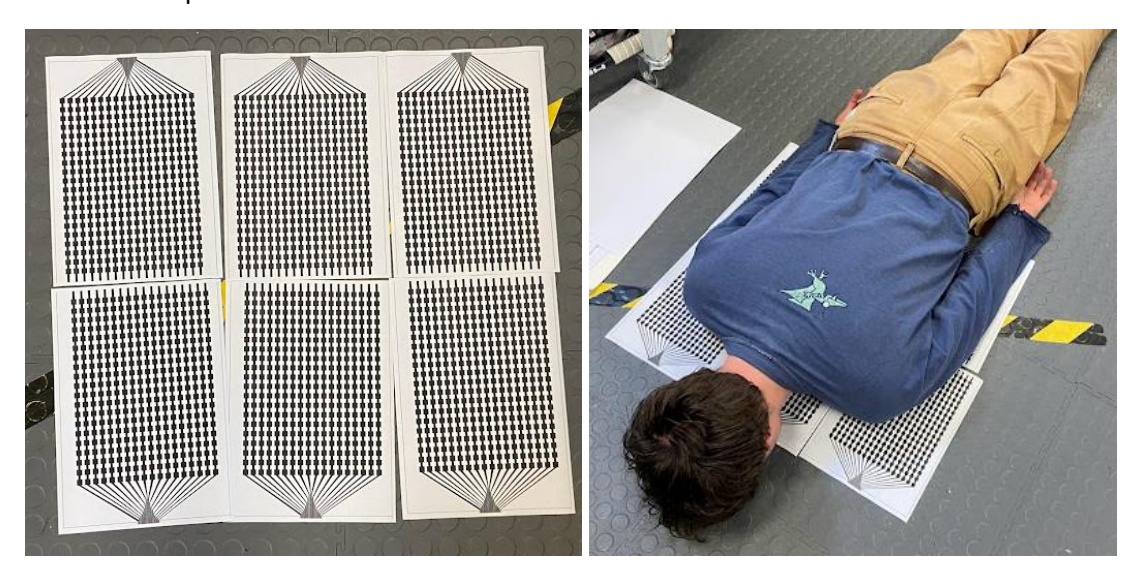


Figure 37 Sizing potential full-size sensor using

Another problem was the cost of the silver ink. A commonly used ink for this application is Loctite ECI 1010 conductive silver ink [55], which cost £220 / 200 g. This was the cheapest available but would consume almost all of the budget allocated for this project (£250). Unfortunately, during the timeframe of this project, no silver ink was available at the University, and no research was being done using the ink, so it was not possible to share the cost.

For manufacturing many (>10) pressure sensors screen printing is the best choice as it scales well with both size and quantity. Hand laying copper tape to make the electrodes was demonstrated successfully here but this is only appropriate as a one-off as the process would become far too labour-intensive.

# 6 Full System Testing

Once the subsystems described in the previous sections were completed, they were integrated to form the full prototype system.

Figure 38 shows a user lying on the completed full-size prototype pressure sensor mat. The data acquisition PCB is running the matrix driving software, and a capture of the pressure map displayed on the user interface is overlaid. This demonstrates the pressure sensor meets the functionality requested in the brief by live outputting the pressure distribution of a user torso lying in the prone position.

The refresh rate of the full-size pressure sensor was ~1 Hz, due to taking the average of 4 readings for every column (9.2 kB/scan). This could be increased but refresh rate was not the most important factor of this project and made the data significantly noisier.

After confirming baseline functionality of the pressure sensor mat, the IPRD vessel was placed under the sensor (uninflated). Figure 39 shows a user lying on the pressure sensor mat on top of the IPRD. This initial prototype IPRD had internal rigid pipes running from the external pneumatic connections to the opposite side of the inflatable. This will be fixed on future IPRD versions, but in this instance was a useful test case to demonstrate that rigid objects underneath the patient cause pressure points which may cause pressure sores to form.

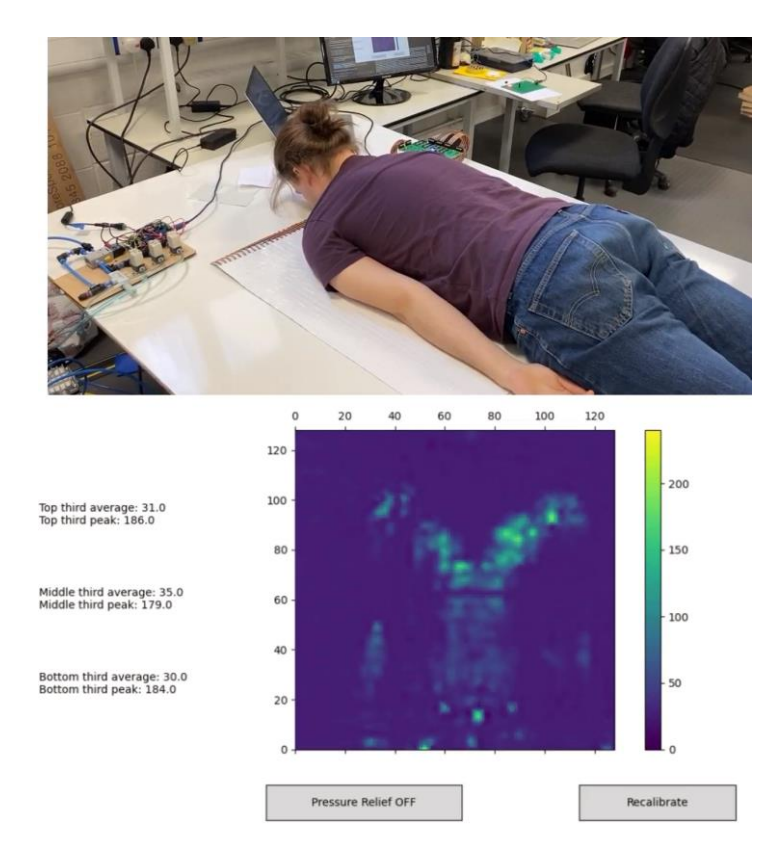


Figure 38 Screen capture from demonstration video 'PressureSensorMat.mp4' demonstrating the function of the pressure sensor mat before being placed on the IPRD. Top: User lying on the pressure mat, Bottom: corresponding pressure map displayed on the user interface simultaneously

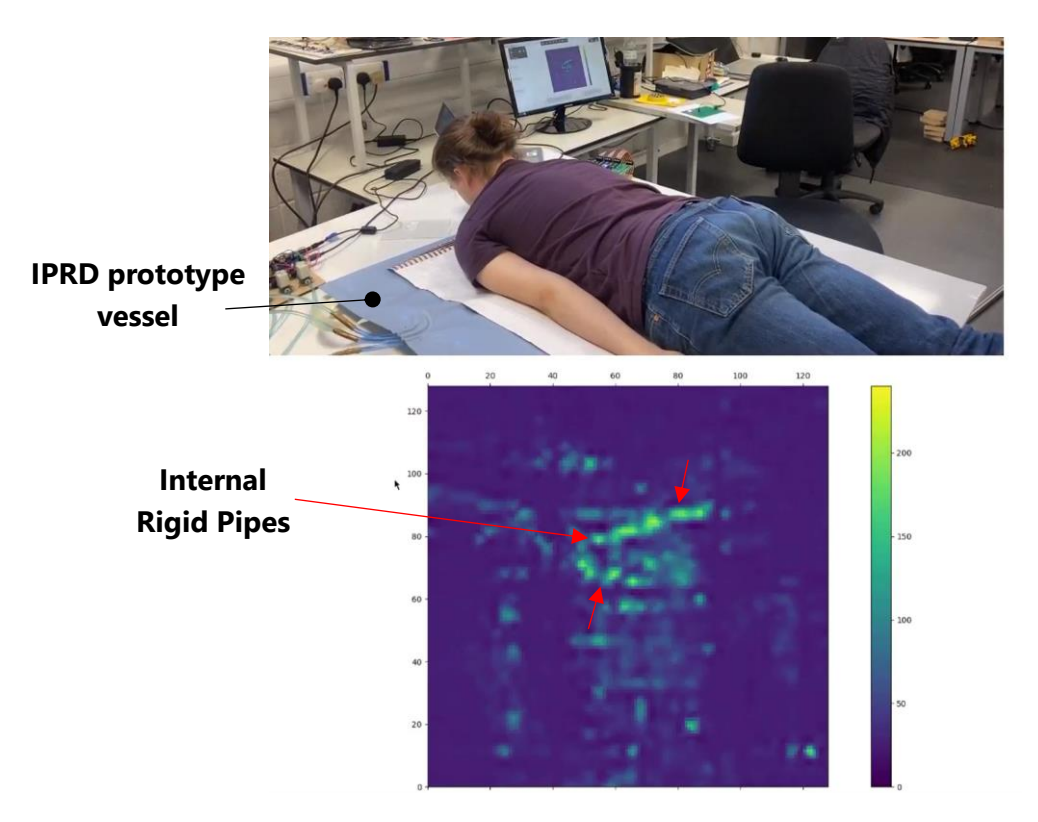


Figure 39 Screen capture from demonstration video 'IPRD\_Uninflated.mp4' demonstrating the function of the pressure sensor placed on the prototype IPRD. Rigid internal tubing is highlighted in the pressure map

Video demonstrations of these tests are included in the Supporting Documents.

## 6.1 Pneumatic Integration

The step of testing the full prototype was to include automatic pneumatic control by sending pressure sensor data to the Arduino controlling the pneumatics (Figure 9). A video of this test is available in the Supporting Documents folder (*IPRD\_InflationFeedback.mp4*).

For this test the sensor was placed on top of the IPRD as before, but the 'pressure relief' mode was toggled in the UI. This activated the automatic pneumatic control code (Figure 30) which averaged each horizontal third of the sensor and inflated corresponding IPRD chambers if any pressures were detected over a threshold. Figure 40 shows a screen-capture from this test.

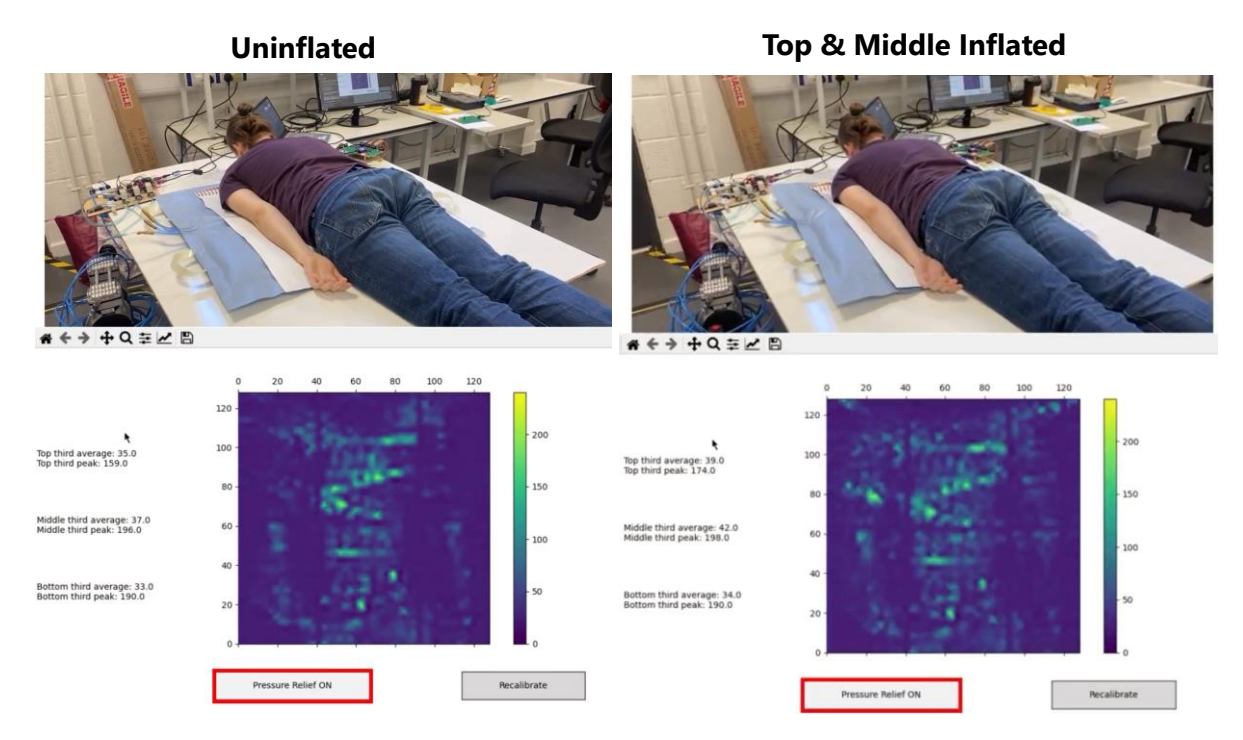


Figure 40 Comparison of pre and post automatic inflation. When the test begins the top and middle sections are over the threshold average pressure (35/255), so these are inflated. After the inflation these average pressures actually increased on the 2 inflated sections.

Figure 40 shows that inflating the top and middle sections increased the average pressure across both, while the pressure on the uninflated bottom section was unchanged. Visually, it can be seen that the general body pressure is slightly more blurred and distributed as the IPRD inflates. The rigid pipes inside the vessel become less defined with inflation, indicating that the patient is cushioned from these objects.

The video demonstration of this test showed that the automatic pneumatic control functioned as intended and inflated sections over the threshold, deflating these if they then fell under the threshold. However, the average data indicates this may not be the best way to implement the automatic pneumatic control. Integrating the pneumatic control with the pressure sensor was completed at the end of the project timeframe, so there was not time to gather user feedback from doctors/nurses that could be used to tune the behaviour of the automatic repositioning, but this is a key improvement that could be added relatively easily given more time.

#### 6.2 Final BOM

A bill of materials for the prototyping activities undertaken is contained in Appendix E. The total cost of all material used in the prototype system was £424 (excluding the IPRD vessel, air compressor, and PC). Most of the pneumatic hardware was repurposed from previous projects so this was saved from the cost, and the air compressor and PC were already available. The total spend for this project was £247.34.

# 7 Conclusions & Future Work

This section compares the performance of the final prototype system against in different scenarios to confirm it meets the brief, and the prototype requirements specification presented previously (Table 6). Future improvements to the pressure sensor system to meet prototype requirements not achieved so far are suggested, as well as outlining potential work packages for improving the capabilities of the pressure sensor and inflatable vessel as further work is done to commercialise the IPRD and integrate a pressure mapping solution.

Table 8 Final prototype test results against original prototype requirement specification (Table 6)

	Requirement	Target Value	Farget Value Achieved value	
1.	Performance			
1.1	Pressure sensor array spatial resolution	< 75 mm spacing	14 mm/cell	PASS
1.2	Pressure sensor covers entire IPRD	800 x 800 mm	680 x 680 mm	Acceptable
1.3	Pressure sensor array sample rate	> 0.3 Hz	Maximum stable rate 1.5 Hz	PASS
1.4	Pressure sensor array accuracy	±5 mmHg (±0.6 kPa)	Not evaluated	Not tested
1.5	Minimum pressure sensor array cell saturation pressure	> 100 mmHg (13 kPa)	Not evaluated	Not tested
1.6	Data output has minimal noise or artefacts that affect true pressure map visibility	Can identify body outline/posture		
1.7	Pressure sensor array does not introduce hard objects to the IPRD surface	No hard/rigid objects in sensor surface	Only flexible thin films use in main construction of pressure sensor mat	PASS
1.8	Pressure sensor array is flexible	Pressure mat can measure pressure on non-flat surfaces (IPRD)	Sensor mat functions when placed on an inflatable	PASS
1.9	Device can automatically reposition based on live pressure mapping data feedback	Closed-loop control of pneumatics achieved	'pressure relief' mode automatically drives pneumatic valves using pressure distribution data	PASS
2.	User			
2.1	Live pressure distribution map can be displayed	Real-time display	Live updating pressure distribution displayed to user	PASS
2.2	Device provides feedback to indicate pressure ulcer formation risk	Audio-visual alerts to healthcare staff	Not implemented	FAIL
2.3	Device can be switched between manual and automatic repositioning easily	User interface allows mode switch	Toggle button for 'pressure relief' mode	PASS
3.	Life in Service			
3.1	Device is modular and sub-systems can be replaced	All sub-systems replaceable	High-level components can be separated (mat/PCB/MCU) Sensor layers cannot be separated	Acceptable
3.2	Pressure sensor is thin and unobtrusive	< 3 mm total thickness	Vinyl (x2): 0.15mm Velostat (x1): 0.1mm Copper (x2): 0.07mm Overall thickness <1mm No rigid components in mat	PASS
3.3	Device can be stored easily by one person	Rolled or folder without damage repeatedly	Sensor mat can be easily disconnected from PCB and rolled or folded flat	PASS

## 7.1 Future Improvements

The first set of improvement work should be to complete any untested or failed requirements from the prototype requirements specification. Table 8 shows that requirements 1.3, 1.4 and 2.2 are untested/fail. 1.3 and 1.4 relate to calibrating the pressure sensor readings so that accurate data (in mmHg or kPa) can be read. 2.2 is a User Interface software feature. As mentioned in the automatic pneumatic control section further user input is required to tune the behaviour of the pneumatic control and this more user interface functionality could be implemented with this as it is not a very big work package.

After fulfilling all of the initial prototype specifications (Table 8) some additional work packages are suggested that would enhance the pressure sensor mat and IPRD capabilities

#### 7.1.1 Sensor Calibration

A feature requested by doctors of the pressure mat is the ability to see calibrated pressure readings (mmHg is often used in medical settings). This would allow them to evaluate the risk of pressure sore formation in real-time and whether repositioning the patient is immediately required. Currently, the pressure map provided shows Arduino voltage readings with a fixed offset taken upon beginning the code. However, Velostat is known to have unreliable pressure vs resistance characteristics and the connection between the copper tape and velostat cannot be assumed perfect across all sensing points [37].

A one-off approach to deal with varying characteristics in the array could be to load each sensing cell individually with a series of known weights and record the output. This would generate a response curve for each sensing cell which could be applied in the visual processing python script to output calibrated pressure readings. This could be achieved with a series of increasing masses, whose footprint fills one sensor cell area, even a handheld force meter to press on each cell. A more sophisticated approach would be to use a CNC controlled 2-axis gantry with a load cell fitted on a vertical axis to press on each sensing cell and record the output curve. The problem with calibrating the mat in this way is that the cell must be pressed in the centre, trying to cover all of sensor cell area, every time. This is difficult with the current prototype because the copper tape was laid by hand so is not perfectly straight, and the vinyl outer layer hides the precise location of the row/column overlapping areas.

However, this approach to calibration would only need to be performed once after constructing the pressure sensor. For a one-off prototype could be done by hand with known masses. For multiple pressure mats it would be necessary to employ a CNC controlled calibration method. This would in turn require the electrodes to be placed much more reliably, which itself would require a better manufacturing method (e.g.: screen-printed electrodes).

#### 7.1.2 Pneumatics Development

The pneumatic hardware presented is suitable for simple uses such as inflating and deflating the IPRD, but adding pressure sensor capabilities opens the door for further developments.

At the moment, pressure sensor data is averaged in horizontal thirds as the IPRD only has three chambers. To take full advantage of the high-resolution pressure sensor an inflatable with more individually controlled chambers could be designed, similar to that presented in Figure 41. This concept uses mechanical drives to reposition the patient, but a similar principle could be applied to IPRD, by designing a larger grid of individually controllable air pockets the patient could be automatically repositioned more effectively by more precisely targeting pressure concentrations. Figure 41 also shows a similar example of how this principle is used in some inflatable wheelchair cushions. These are not individually controllable pockets, but the shape of the inflatable allows it to conform to the patients more.

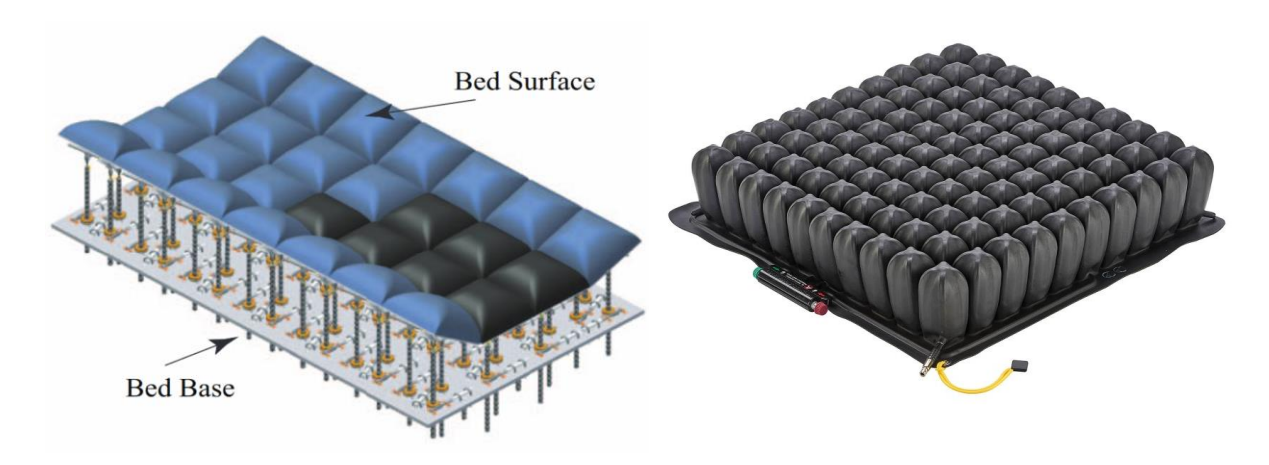


Figure 41 Example of alternative pneumatic vessel design.

Left: air cushioned hospital bed concept with many air 'bladders' to support the patient and allow higher resolution control of automatic repositioning - image from Yousefi (2011)[14]

Right: Inflatable wheelchair cushion with many inflating pockets which conform the patient [56]

Another area that can be improved is the pneumatic control hardware, which can be altered to provide more functionality and performance.

A quick performance increase can be found by replacing the vacuum generator used to deflate the IRPD. A Festo VN10 LT3 Venturi vacuum generator is currently being used which has a 62 L/min suction rate (and a 1 mm diameter Laval nozzle[57]). Festo offer a direct replacement that has a 3 mm Laval nozzle that increases the suction rate 5x to 300 L/min for the same 4 Bar air supply. Since the vacuum generator is only used to suction the air vessel it makes sense to use a vacuum generator more capable for this, since currently it is very slow to empty the bag of air via pneumatic control.

Another improvement can be made to the pneumatic control architecture. Currently, the chambers in the IPRD vessel are either in a state of inflation, vacuuming, or closed due to the pneumatic valves used (Figure 29). To allow automatic repositioning algorithms, and nurses/doctors more control the IPRD, the hardware can be altered to allow passive emptying of the air vessel to atmospheric pressure. A potential new schematic is given in Figure 42, using 3/2 and 5/3 solenoids to offer more control over the inflation 'states' of each vessel chamber.

This redesign would give the automatic pneumatic control algorithm another option when repositioning patients. At the moment, the vessel is inflated and deflated in open-loop control – there is no way of knowing how much air is in the bag. If the vessel is intermittently normalised to atmospheric pressure as a datum, then the pneumatic control algorithm knows how much air is in vessel at any point from then on.

Additionally, this redesign also enables passive pressure release to create a rippling effect. The current pneumatic hardware only allows either vacuum or pressure into a chamber at once; two different chambers cannot be vacuuming and inflating respectively at the same time. The new pneumatics in Figure 42 would allow a chamber to be draining to atmospheric pressure while another is inflating simultaneously.

#### REVISED IPRD PNEUMATIC CONTROL

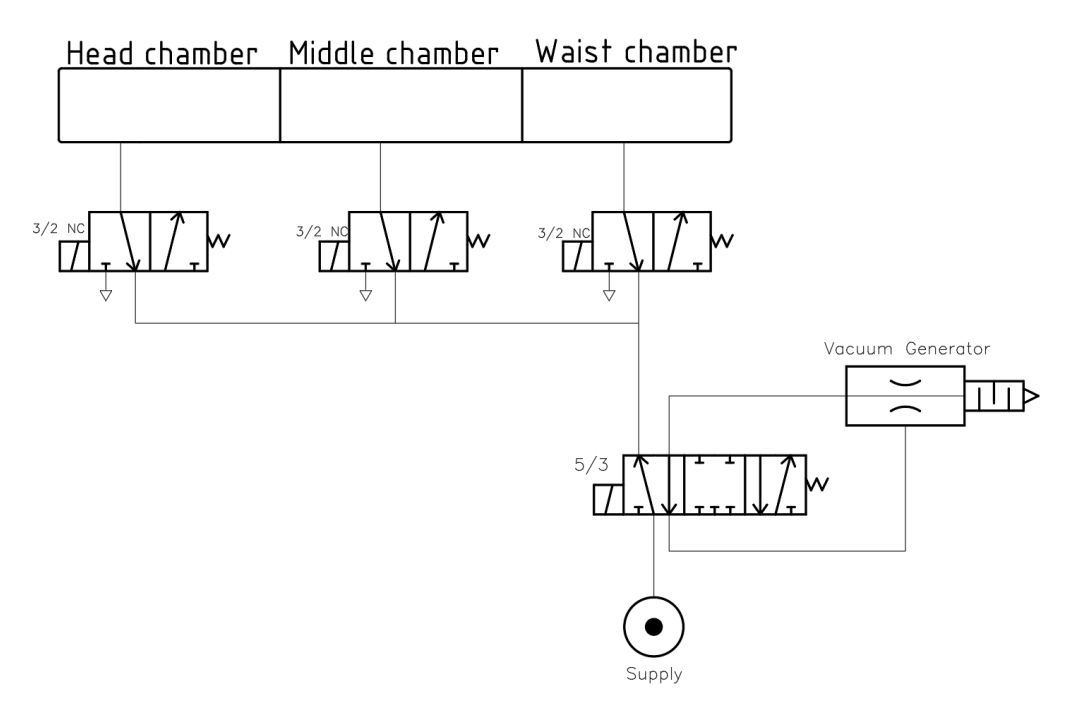


Figure 42 Alternative IPRD pneumatic control architecture. Utilising 5/3 and 3/2 solenoids to allow passive draining to atmosphere, as well as simultaneous inflation/draining of different chambers

#### 7.1.3 Electronics Improvements

Prototyping work in this project is nearing the performance limits of an Arduino when scanning such a large array so fast and sending all of the data over the serial port and further developments could consider higher performance alternatives.

One better approach is to replace the Arduino with an FPGA (field programmable gate array). FPGAs are more expensive and much harder to program than an Arduino but provide much higher performance and are suited extremely well to this application. FPGAs can have hundreds of IO ports and excel in parallel processing and precise timing applications. A good example of using an FPGA to drive a large pressure sensor array is Cheng et al., (2016)[58]. The authors similarly use fast response analog switches to switch a low-noise power source to the rows of the array, but control these from an FPGA, which also has internal 24-bit ADCs and signal processing on the input lines. The data stream is then sent via UART-USB to a PC. Ultimately, they are able to scan a 128 x 128 matrix at 40 Hz, with 24-bit precision, a massive improvement over the performance of the prototype developed for this project.

However, fast refresh rates (> 10Hz) and increasing the array size and resolution beyond what has been developed for this project is arguably unnecessary based on the current needs of the IPRD project. Any further electrical developments should weigh-up whether the increased complexity, cost and development time is worth it with respect to the current needs of the project.

#### 7.1.4 Electrode Improvements

As detailed in Section 5.3, screen-printed electrodes are a key for developing the pressure sensor from a handmade one-off to a manufacturable assembly. However, there are some more considerations above simply printing conductive silver ink on to PET.

Cutting holes into the electrode sheet between the sensing cells has successfully been demonstrated to make the mat more conformable and reduce 'hammocking' (where the mat stretches across a depression – reading anomalously high pressures as a result) and creases that occur when pressing thin films into soft surfaces.

Sundaram et al., (2019)[34] demonstrate an auxetic electrode substrate pattern (Figure 43) that can stretch and fold despite being constructed from inextensible materials. Additionally, one of the leading pressure sensor manufacturers, Tekscan, advertise the ConforMat on their website (Figure 43) which uses a similar cut patter to allow the mat to conform into soft cushions. An interesting future test for this project could be laser-cut screen-printed electrodes that can be bonded more tightly to the surface of the inflatable. Bonding the pressure sensor to the surface will reduce creasing or hammocking causing anomalous data that might trip up automatic repositioning algorithms or misinform nurses.



Figure 43 Left: Auxetic electrode/substrate pattern demonstrated in Sundaram (2019) [34] Right: Tekscan ConforMat designed to conform into soft wheelchair cushions to avoid hammocking [59]

Finally, future research into biocompatible, washable casing materials for the electrodes and substrate will also be required. This is to protect the internal layers of the mat from moisture and allow removal for washing to prevent transfer of disease between ICU patients.

#### 7.2 Final Conclusions

Overall, this project has met the original brief request of developing a pressure sensor mat which can be placed on the Inflatable Prone Repositioning Device (IPRD) and feedback live pressure distribution data to doctors or nurses. A full-size prototype sensor array was created with 15 mm/cell resolution over a 70 x 70cm which was sufficient to cover the top surface of the IPRD. Testing the pressure sensor in a prone position successfully demonstrated that the body outline could be made out, and that local pressure points could be identified. Additionally testing with a prototype version of the IPRD vessel underneath showed that internal tubing caused pressure concentration points which may lead to pressure sores if left unchecked.

Going beyond the original brief, it was also demonstrated that the live pressure sensor data could be used to automatically control the pneumatic valves to reposition the patient with no manual input. Although the effect of this was limited and continued user feedback with healthcare professionals is required to develop the automatic control algorithm.

The successfully prototyping activities from this project can be carried forward, and several potential areas have been highlighted as key future improvements to develop the pressure sensor into a more technologically advanced product that can be seamlessly integrated with the IPRD:

- Improving automatic pneumatic control algorithms to reposition patients constantly.
- Implementing sensor calibration methods to provide pressure data in mmHg.
- Improving sensor driving electronics.
- Implementing a biocompatible, washable casing suitable for an ICU environment.
- Testing novel methods of electrode construction to all the pressure sensor to conform with the inflatable vessel.

# References

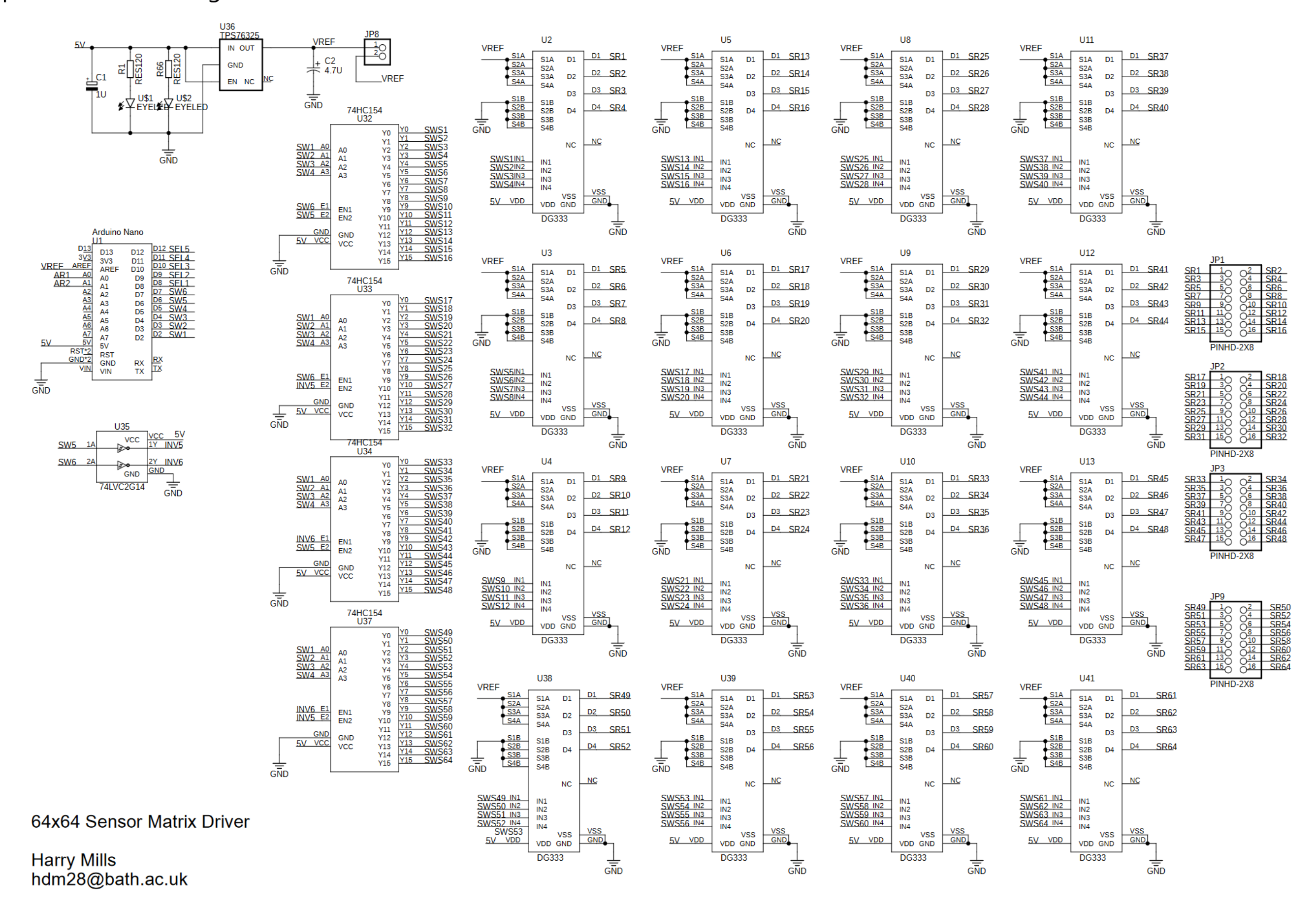
- [1] C. Guérin *et al.*, 'Prone position in ARDS patients: why, when, how and for whom', *Intensive Care Med*, vol. 46, no. 12, pp. 2385–2396, 2020, doi: 10.1007/s00134-020-06306-w.
- [2] M. Diamond, H. L. Peniston, D. K. Sanghavi, and S. Mahapatra, 'Acute Respiratory Distress Syndrome', in *StatPearls*, Treasure Island (FL): StatPearls Publishing, 2024. Accessed: Apr. 25, 2024. [Online]. Available: http://www.ncbi.nlm.nih.gov/books/NBK436002/
- [3] 'Acute respiratory distress syndrome (ARDS)', nhs.uk. Accessed: Apr. 25, 2024. [Online]. Available: https://www.nhs.uk/conditions/acute-respiratory-distress-syndrome/
- [4] National Clinical Guideline Centre (UK), *The Prevention and Management of Pressure Ulcers in Primary and Secondary Care.* in National Institute for Health and Care Excellence: Guidelines. London: National Institute for Health and Care Excellence (NICE), 2014. Accessed: Nov. 06, 2023. [Online]. Available: http://www.ncbi.nlm.nih.gov/books/NBK248068/
- [5] H. Kirkland-Walsh, O. Teleten, M. Wilson, and B. Raingruber, 'Pressure Mapping Comparison of Four OR Surfaces', *AORN J*, vol. 102, no. 1, p. 61.e1–9, Jul. 2015, doi: 10.1016/j.aorn.2015.05.012.
- [6] Nursing Times, 'Pressure ulcer education 5 keeping patients moving', Nursing Times. Accessed: Apr. 26, 2024. [Online]. Available: https://www.nursingtimes.net/clinical-archive/tissue-viability/pressure-ulcer-education-5-keeping-patients-moving-13-01-2020/
- [7] C. Dealey, J. Posnett, and A. Walker, 'The cost of pressure ulcers in the United Kingdom', *J Wound Care*, vol. 21, no. 6, pp. 261–262, 264, 266, Jun. 2012, doi: 10.12968/jowc.2012.21.6.261.
- [8] J. Heikenfeld *et al.*, 'Wearable sensors: modalities, challenges, and prospects', *Lab Chip*, vol. 18, no. 2, pp. 217–248, Jan. 2018, doi: 10.1039/C7LC00914C.
- [9] 'Mattress Pressure Mapping | Matrix Based Tactile Force Sensor | Human Body Interface Pressure Mapping | Body Pressure Mapping'. Accessed: Nov. 09, 2023. [Online]. Available: https://www.sensorprod.com/dynamic/mattress.php
- [10] 'Body Pressure Distribution | Body Pressure Measurement System (BPMS) Research | Tekscan'. Accessed: Nov. 07, 2023. [Online]. Available: https://www.tekscan.com/products-solutions/systems/body-pressure-measurement-system-bpms-research
- [11] 'XSENSOR | Patient Bed Monitoring'. Accessed: Nov. 09, 2023. [Online]. Available: https://www.xsensor.com/solutions-and-platform/csm/patient-bed-monitoring
- [12] M. Yip, D. Da He, E. Winokur, A. G. Balderrama, R. Sheridan, and H. Ma, 'A flexible pressure monitoring system for pressure ulcer prevention', *Annu Int Conf IEEE Eng Med Biol Soc*, vol. 2009, pp. 1212–1215, 2009, doi: 10.1109/IEMBS.2009.5333964.
- [13] B. Mutlu, A. Krause, J. Forlizzi, C. Guestrin, and J. Hodgins, 'Robust, low-cost, non-intrusive sensing and recognition of seated postures', in *Proceedings of the 20th annual ACM symposium on User interface software and technology*, in UIST '07. New York, NY, USA: Association for Computing Machinery, Oct. 2007, pp. 149–158. doi: 10.1145/1294211.1294237.
- [14] R. Yousefi *et al.*, 'A smart bed platform for monitoring & Ulcer prevention', in *2011 4th International Conference on Biomedical Engineering and Informatics (BMEI)*, Oct. 2011, pp. 1362–1366. doi: 10.1109/BMEI.2011.6098589.
- [15] S. Caggiari, L. Jiang, D. Filingeri, and P. Worsley, 'Optimization of Spatial and Temporal Configuration of a Pressure Sensing Array to Predict Posture and Mobility in Lying', *Sensors (Basel)*, vol. 23, no. 15, p. 6872, Aug. 2023, doi: 10.3390/s23156872.

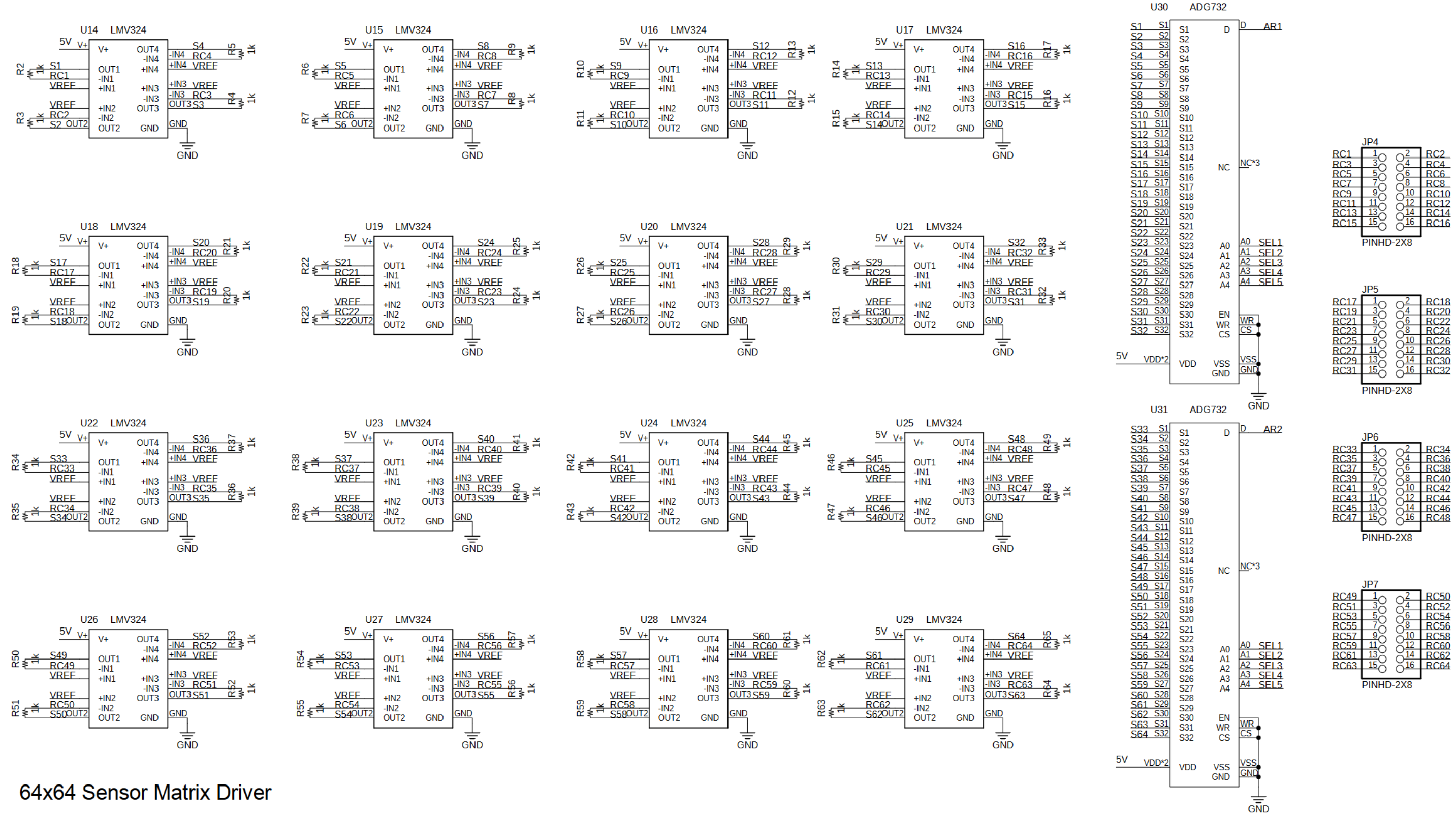
- [16] H. Mills, 'Inflation Proning Repositioning Device (IPRD) Major Individual Design Project: Initial Brief'. University of Bath, Oct. 2023.
- [17] T. P. D. A. Barros, J. M. X. N. Teixeira, W. F. M. Correia, and A. E. F. Da Gama, 'Velostat-Based Pressure Sensor Matrix for a Low-Cost Monitoring System Applied to Prevent Decubitus Ulcers', in *XXVII Brazilian Congress on Biomedical Engineering*, T. F. Bastos-Filho, E. M. de Oliveira Caldeira, and A. Frizera-Neto, Eds., in IFMBE Proceedings. Cham: Springer International Publishing, 2022, pp. 835–842. doi: 10.1007/978-3-030-70601-2\_126.
- [18] P. Chung, A. Rowe, M. Etemadi, H. Lee, and S. Roy, 'Fabric-based Pressure Sensor Array for Decubitus Ulcer Monitoring', *Conf Proc IEEE Eng Med Biol Soc*, vol. 2013, pp. 6506–6509, 2013, doi: 10.1109/EMBC.2013.6611045.
- [19] Adafruit, 'Conductive Rubber Sheet / Stretch Sensor- 200mm x 200mm x 1mm'. Accessed: Nov. 08, 2023. [Online]. Available: https://www.adafruit.com/product/5463
- [20] L. Jabban, B. Metcalfe, D. Zhang, and P. Iravani, 'Pressure Sensitive Skin for Prosthetic Hands: 2D Contact Location Determination Using Output Connections from a Single Side', in *2020 42nd Annual International Conference of the IEEE Engineering in Medicine & Biology Society (EMBC)*, Montreal, QC, Canada: IEEE, Jul. 2020, pp. 4341–4344. doi: 10.1109/EMBC44109.2020.9176163.
- [21] K.-H. Kim, S. K. Hong, N.-S. Jang, S.-H. Ha, H. W. Lee, and J.-M. Kim, 'Wearable Resistive Pressure Sensor Based on Highly Flexible Carbon Composite Conductors with Irregular Surface Morphology', *ACS Appl. Mater. Interfaces*, vol. 9, no. 20, pp. 17499–17507, May 2017, doi: 10.1021/acsami.7b06119.
- [22] C. Metzger *et al.*, 'Flexible-foam-based capacitive sensor arrays for object detection at low cost', *Applied Physics Letters*, vol. 92, no. 1, p. 013506, Jan. 2008, doi: 10.1063/1.2830815.
- [23] M. Hopkins, R. Vaidyanathan, and A. H. Mcgregor, 'Examination of the Performance Characteristics of Velostat as an In-Socket Pressure Sensor', *IEEE Sensors J.*, vol. 20, no. 13, pp. 6992–7000, Jul. 2020, doi: 10.1109/JSEN.2020.2978431.
- [24] 'Welcome to Processing!', Processing. Accessed: Apr. 27, 2024. [Online]. Available: https://processing.org//
- [25] 'Visualization with Arduino and Processing'. Accessed: Apr. 27, 2024. [Online]. Available: https://www.arduino.cc/education/visualization-with-arduino-and-processing/
- [26] A. S. Fiorillo, C. D. Critello, and S. A. Pullano, 'Theory, technology and applications of piezoresistive sensors: A review', *Sensors and Actuators A: Physical*, vol. 281, pp. 156–175, Oct. 2018, doi: 10.1016/j.sna.2018.07.006.
- [27] T. D'Alessio, 'Measurement errors in the scanning of piezoresistive sensors arrays', *Sensors and Actuators A: Physical*, vol. 72, no. 1, pp. 71–76, Jan. 1999, doi: 10.1016/S0924-4247(98)00204-0.
- [28] J.-S. Kim, D.-Y. Kwon, and B.-D. Choi, 'High-Accuracy, Compact Scanning Method and Circuit for Resistive Sensor Arrays', *Sensors*, vol. 16, no. 2, Art. no. 2, Feb. 2016, doi: 10.3390/s16020155.
- [29] 'CD4051BQPWRQ1 Texas Instruments | Mouser', Mouser Electronics. Accessed: Apr. 27, 2024. [Online]. Available: https://www.mouser.co.uk/ProductDetail/Texas-Instruments/CD4051BQPWRQ1?qs=YxwvVpIHM%2FImKeVzaclE6Q%3D%3D
- [30] W. E. Snyder and J. St. Clair, 'Conductive Elastomers as Sensor for Industrial Parts Handling Equipment', *IEEE Trans. Instrum. Meas.*, vol. 27, no. 1, pp. 94–99, 1978, doi: 10.1109/TIM.1978.4314628.
- [31] D. Prutchi and M. Arcan, 'Dynamic contact stress analysis using a compliant sensor array', *Measurement*, vol. 11, no. 3, pp. 197–210, Jun. 1993, doi: 10.1016/0263-2241(93)90039-K.
- [32] H. Liu, Y.-F. Zhang, Y.-W. Liu, and M.-H. Jin, 'Measurement errors in the scanning of resistive sensor arrays', *Sensors and Actuators A: Physical*, vol. 163, no. 1, pp. 198–204, Sep. 2010, doi: 10.1016/j.sna.2010.08.004.

- [33] R. S. Saxena, R. K. Bhan, and A. Aggrawal, 'A new discrete circuit for readout of resistive sensor arrays', *Sensors and Actuators A: Physical*, vol. 149, no. 1, pp. 93–99, Jan. 2009, doi: 10.1016/j.sna.2008.10.013.
- [34] S. Sundaram, P. Kellnhofer, Y. Li, J.-Y. Zhu, A. Torralba, and W. Matusik, 'Learning the signatures of the human grasp using a scalable tactile glove', *Nature*, vol. 569, no. 7758, Art. no. 7758, May 2019, doi: 10.1038/s41586-019-1234-z.
- [35] L. Spreeuwers and H. Wang, 'A high resolution pressure sensor for measurement of grip force', presented at the 40th WIC Symposium on Information Theory in the Benelux 2019, May 2019. Accessed: Nov. 05, 2023. [Online]. Available: https://research.utwente.nl/en/publications/a-high-resolution-pressure-sensor-formeasurement-of-grip-force
- [36] 'What is the virtual short of an op-amp? | Toshiba Electronic Devices & Storage Corporation | Europe(EMEA)'. Accessed: Apr. 28, 2024. [Online]. Available: https://toshiba.semicon-storage.com/eu/semiconductor/knowledge/faq/linear\_opamp/what-is-the-virtual-short-of-an-op-amp.html
- [37] *Hi-Res Pressure Sensor Matrix with the LattePanda*, (Sep. 19, 2017). Accessed: Nov. 07, 2023. [Online Video]. Available: https://www.youtube.com/watch?v=4JBSHqUcaG4
- [38] 'TPS763 data sheet, product information and support | Tl.com'. Accessed: Apr. 28, 2024. [Online]. Available: https://www.ti.com/product/TPS763?qgpn=tps763
- [39] 'DG333A, DG333AL Analog Switches and Multiplexers Quality | Vishay'. Accessed: Apr. 29, 2024. [Online]. Available: https://www.vishay.com/en/product/70803/tab/quality/
- [40] 'CD74HC154 data sheet, product information and support | Tl.com'. Accessed: Apr. 29, 2024. [Online]. Available: https://www.ti.com/product/CD74HC154
- [41] 'SN74LVC2G14 data sheet, product information and support | Tl.com'. Accessed: Apr. 29, 2024. [Online]. Available: https://www.ti.com/product/SN74LVC2G14
- [42] 'LMV324 data sheet, product information and support | Tl.com'. Accessed: Apr. 29, 2024. [Online]. Available: https://www.ti.com/product/LMV324#description
- [43] 'ADG732 Datasheet and Product Info | Analog Devices'. Accessed: Apr. 29, 2024. [Online]. Available: https://www.analog.com/en/products/adg732.html
- [44] 'PCB Design Layout Guidelines for Engineers'. Accessed: Apr. 29, 2024. [Online]. Available: https://resources.pcb.cadence.com/blog/2023-pcb-design-layout-guidelines-for-engineers
- [45] 'JLCPCB'. Accessed: Apr. 29, 2024. [Online]. Available: https://cart.jlcpcb.com/quote
- [46] 'China PCB Prototype & Fabrication Manufacturer PCB Prototype the Easy Way'. Accessed: Apr. 29, 2024. [Online]. Available: https://www.pcbway.com/
- [47] 'Fast sampling from analog input Yet Another Arduino Blog', Fast sampling from analog input Yet Another Arduino Blog. Accessed: Apr. 27, 2024. [Online]. Available: http://yaab-arduino.blogspot.com/2015/02/fast-sampling-from-analog-input.html
- [48] 'Arduino PortManipulation | Arduino Documentation'. Accessed: Apr. 29, 2024. [Online]. Available: https://docs.arduino.cc/retired/hacking/software/PortManipulation/
- [49] 'ADS8327 data sheet, product information and support | Tl.com'. Accessed: Apr. 29, 2024. [Online]. Available: https://www.ti.com/product/ADS8327
- [50] L. Ortlieb, 'Repositioning of Intensive Care Patients in the Prone Position'. University of Bath, May 2023.
- [51] A. Vangsgaard, 'Design of Device to Improve the Repositioning of Proning Patients'. University of Bath, May 2022.

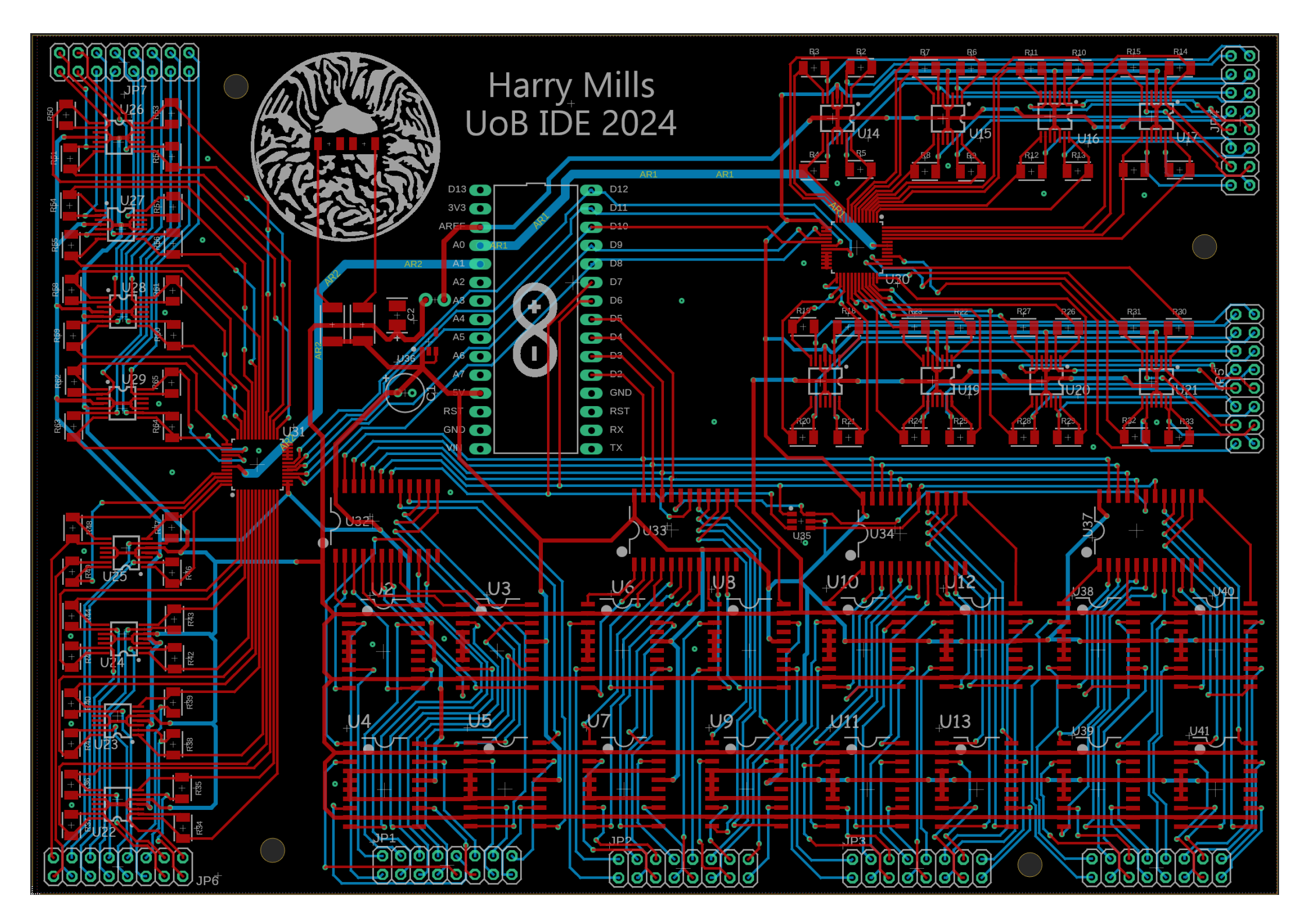
- [52] 'Premium Gloss: White » CWS', CWS. Accessed: Apr. 30, 2024. [Online]. Available: https://carwrapsupplier.co.uk/product/gloss-white/
- [53] '65801-016LF | Clincher<sup>TM</sup> | Amphenol'. Accessed: Apr. 30, 2024. [Online]. Available: https://www.amphenol-cs.com/product/65801016lf.html
- [54] Z. M. Tsikriteas, 'Screen Printing Instructions'. University of Bath, Mar. 05, 2024.
- [55] 'LOCTITE® ECI 1010 E&C, 236,81 €', LOCTITE® ECI 1010 E&C, 236,81 €. Accessed: Apr. 30, 2024. [Online]. Available: https://print-your-electronics-with-loctite.com/LOCTITEZ-ECI-1010-E-C
- [56] 'Roho Quadtro High Profile Pressure Cushion | Hospital Beds'. Accessed: May 01, 2024. [Online]. Available: https://www.hospitalbeds.co.uk/roho-quadtro-select-high-profile-pressure-relief-cushion.html
- [57] 'Buy Vacuum generator, pneumatic VN online | Festo TW'. Accessed: May 01, 2024. [Online]. Available: https://www.festo.com/tw/en/p/vacuum-generator-pneumatic-id\_VN/?q=%7E%3AsortByCoreRangeAndSp2020
- [58] J. Cheng, M. Sundholm, B. Zhou, M. Hirsch, and P. Lukowicz, 'Smart-surface: Large scale textile pressure sensors arrays for activity recognition', *Pervasive and Mobile Computing*, vol. 30, pp. 97–112, Aug. 2016, doi: 10.1016/j.pmcj.2016.01.007.
- [59] 'Seating Design & Testing | Wheelchair Pressure Mapping | CONFORMat System | Tekscan'. Accessed: May 01, 2024. [Online]. Available: https://www.tekscan.com/products-solutions/systems/conformat-system

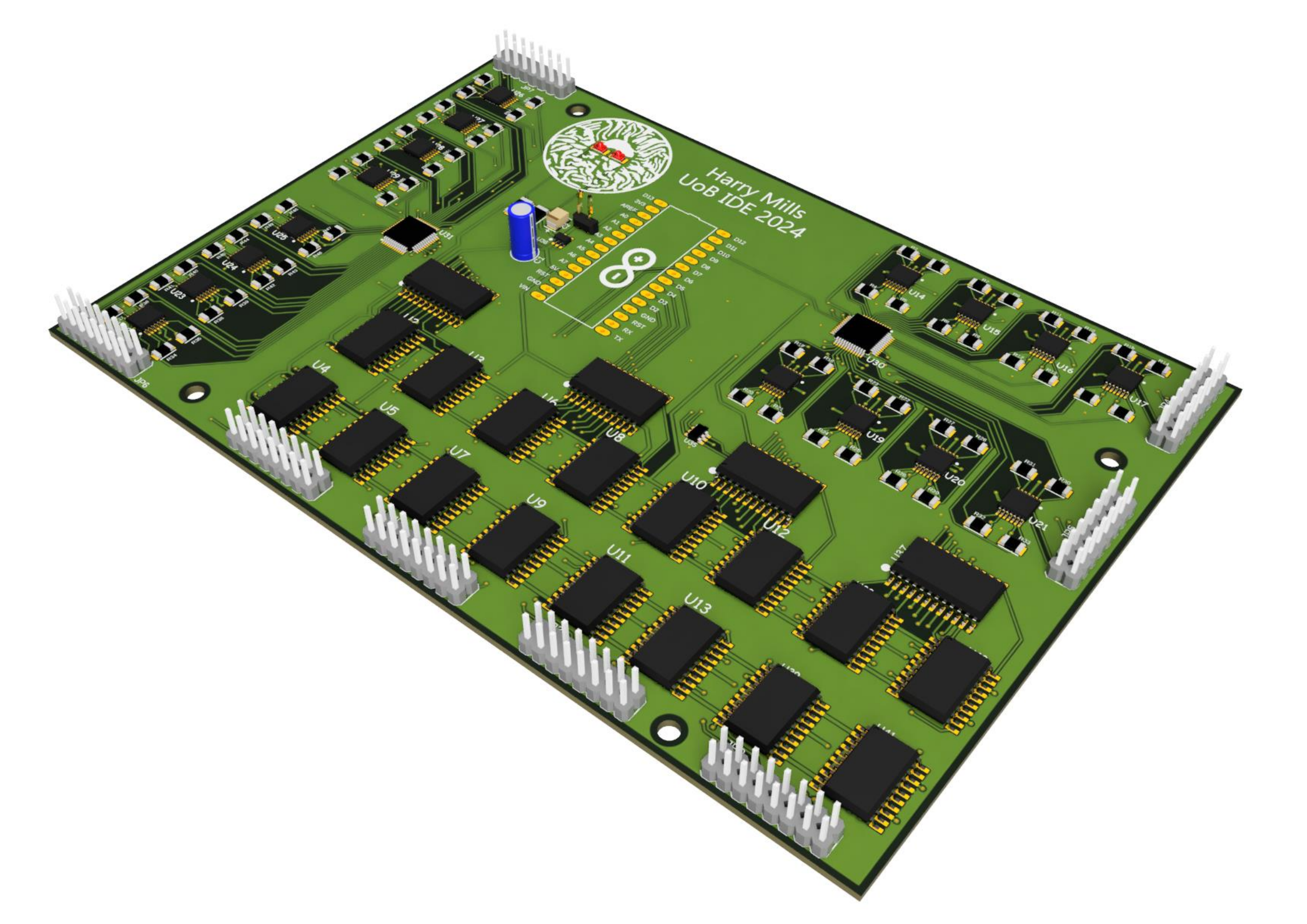
# Appendix A: PCB Design Documents



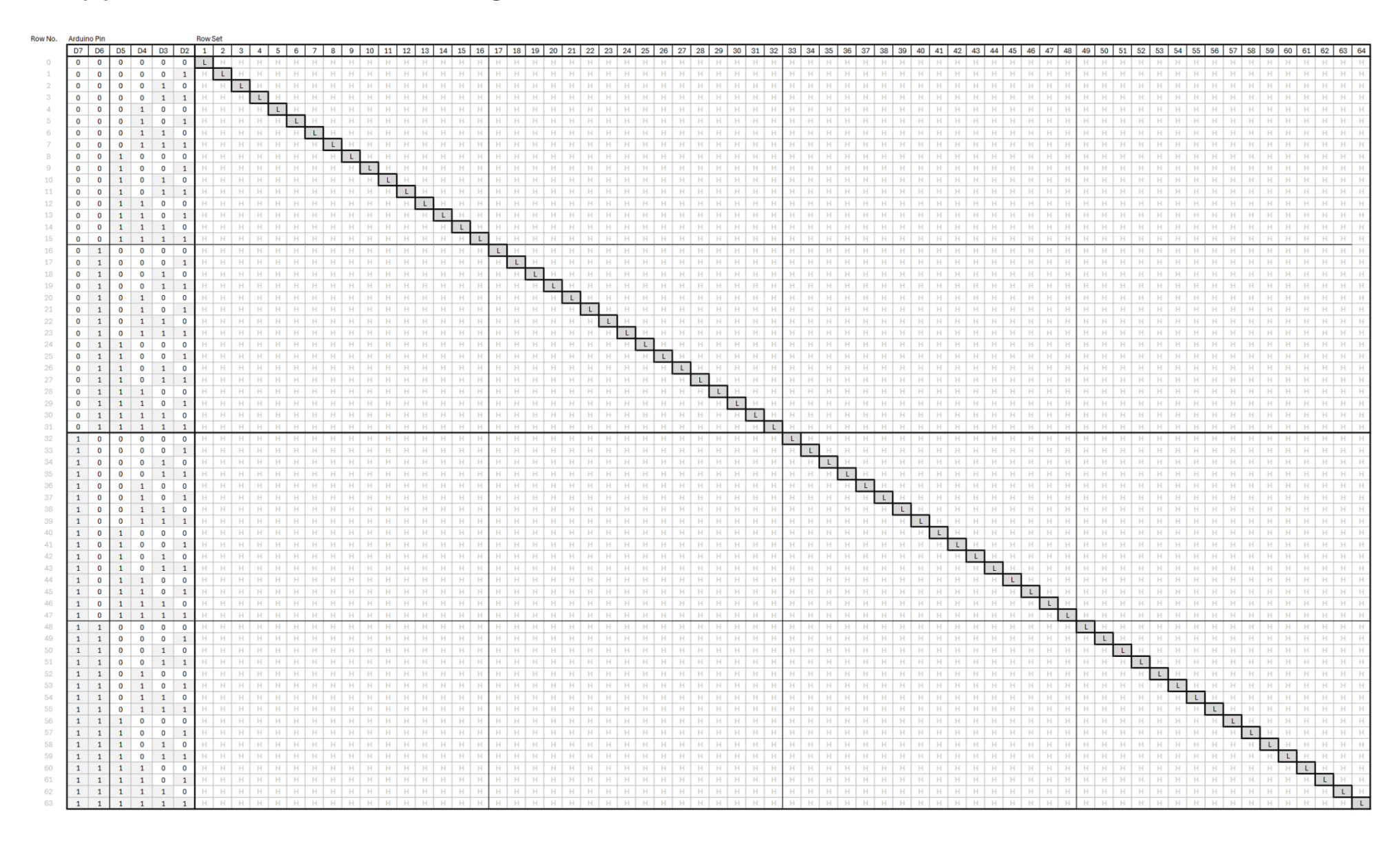


Harry Mills hdm28@bath.ac.uk





# Appendix B: Row Control Logic Truth Table



# Appendix C: Arduino ADC Clock Pre-scale Modification

```
#define cbi(sfr, bit) (_SFR_BYTE(sfr) &= ~_BV(bit))
#define sbi(sfr, bit) (_SFR_BYTE(sfr) |= _BV(bit))

void setup()
{
   sbi(ADCSRA, ADPS2);
   cbi(ADCSRA, ADPS1);
   cbi(ADCSRA, ADPS0);
   ...
```

Figure 44 Arduino code addition to set ADC clock to 1 MHz

The above code [47] modifies the pre-scale factor from 128 to 16 to give an 8x increase in sample speed.

# Appendix D: Screen Printed Electrode Design

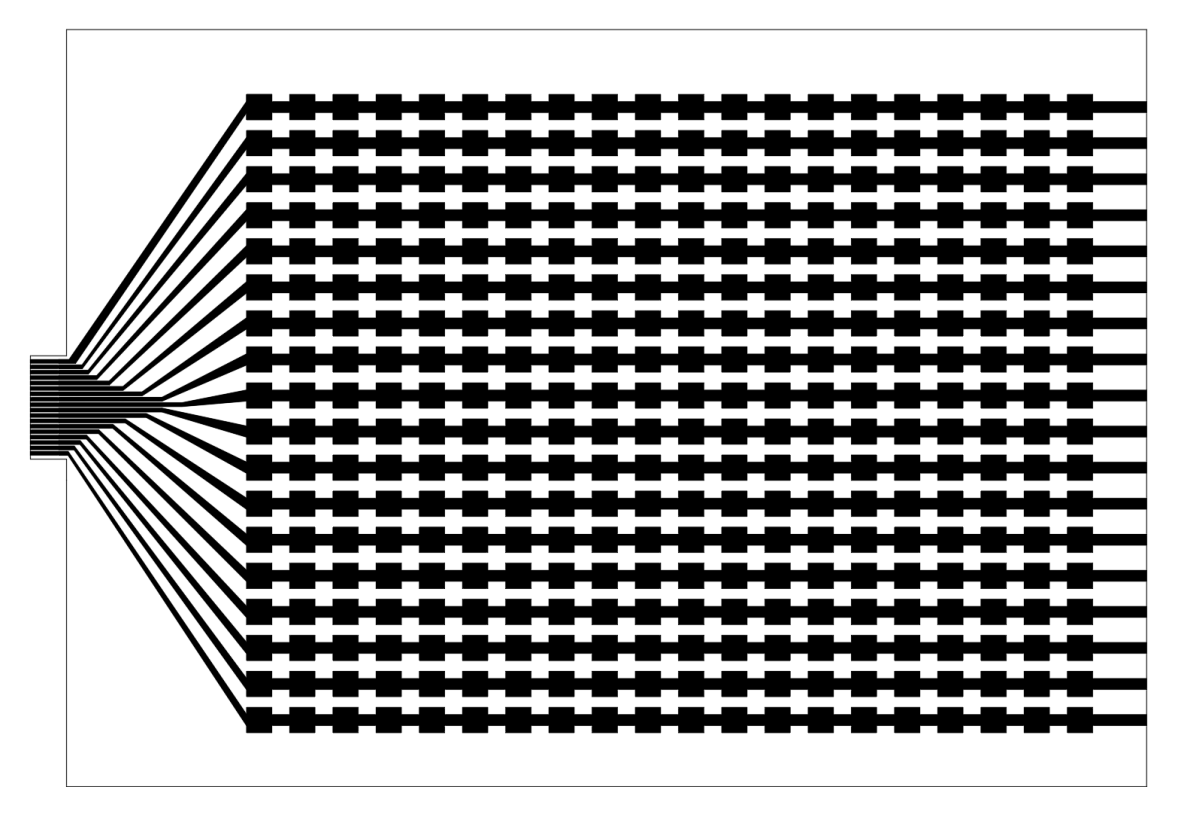


Figure 45 Iteration 1

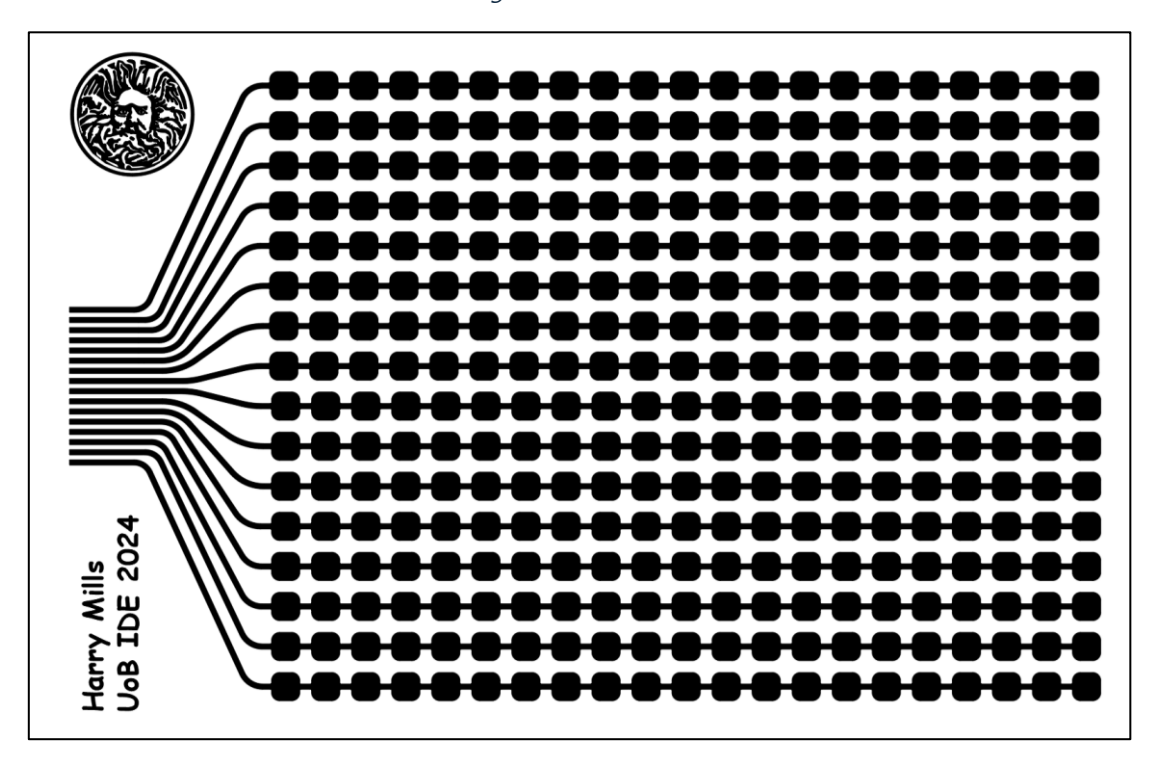


Figure 46 Iteration 2

# Appendix E: Prototype System Bill of Materials

Bill of Materials											
Sub-System	tem Part No. Description		Unit C	Unit Cost (£)		Supplier	Cost (£)		Supplier Part No.	1	
	1	Digital Acquisition PCB (Blank)	£	7.00	1	JLCPCB	£	7.00	-	1	
ē	2	Arduino Nano Clone (ATMega 328P)	£	18.00	1	Farnell	£	18.00	1848691		
Hardware 3)	3	16:1 Demultiplexer CD74HC154	£	0.53	4	Mouser	£	2.12	595-CD74HC154M96		
ırd	4	2.5 V LDO Regulator	£	0.54	1	Mouser	£	0.54	595-TPS76325DBVR		
H <sub>2</sub>	5	4.7uF Capacitor (Tantalum)	£	0.50	1	Mouser	£	0.50	80-T494B475K016		
Digital Acquisition H (DAQ PCB)	6	Quad SPDT analog switch IC ADG333A	£	5.92	16	Farnell	£	94.72	4022127		
sitio	7	Dual inverter logic gate IC 74LVC2G14	£	0.19	1	Farnell	£	0.19	2463880		
duis AC	8	Red LED (3216 SMD)	£	0.63	2	Farnell	£	1.26	3605890		
) (D	9	390 ohm resistor (5025 SMD)	£	0.11	2	Farnell	£	0.22	2861700		
al /	10	1 kohm resistor (3216 SMD)	£	0.01	64	Farnell	£	0.92	2447473		
gita	11	Quad op-amp IC LMV324	£	0.49	16	Farnell	£	7.87	1842586		
Θ	12	32:1 Analog Multiplexer ADG732	£	11.29	2	Farnell	£	22.58	4032557		PCB TOTAL:
	13	16 pin (2 row) header pins	£	0.12	8	Farnell	£	0.97	1593445	£	156.89
at	14	Vinyl car wrap sheet (1 x 1.5m)	£	20.00	1	Amazon	£	20.00	-		
Ž	15	Copper tape 6mm wide 20m roll	£	5.00	5	Amazon	£	25.00	-		
Sensor Mat	16	16 pin ribbon cable (1.27mm pitch, 5m)	£	8.00	1	Amazon	£	8.00	-		
Sue	17	16 pin IDC connector	£	0.42	8	Farnell	£	3.36	2843498		MAT TOTAL:
Š	18	Velostat sheet (30 x 30cm)	£	4.87	7	Adafruit	£	34.09	1361	£	90.45
ပ	19	2/2 NC Solenoid valves (24V)	£	26.03	3	RS	£	78.09	892-9993		
iati rol	20	5/2 Solenoid valve (24V)	£	9.19	1	Amazon	£	9.19	-		
Pneumatic Control	21	Vacuum generator -0.89 Bar	£	35.34	1	RS	£	35.34	202-2417		
ne Co	22	Arduino Mega	£	35.50	1	RS	£	35.50	715-4084		PNEU TOTAL:
₾.	23	Arduino relay shield v3.0 (SeeedStudio)	£	18.95	1	RS	£	18.95	174-3234	£	177.07
									Grand Total:	£	424.41